

Dynamics of magma ascent in the volcanic conduit

Helge M. Gonnermann and Michael Manga

Overview

This chapter presents the various mechanisms and processes that come into play within the volcanic conduit for a broad range of effusive and dry explosive volcanic eruptions. Decompression during magma ascent causes volatiles to exsolve and form bubbles containing a supercritical fluid phase. Viscous magmas, such as rhyolite or crystal-rich magmas, do not allow bubbles to ascend buoyantly and may also hinder bubble growth. This can lead to significant gas overpressure and brittle magma fragmentation. During fragmentation in vulcanian, subplinian, and plinian eruptions, gas is released explosively into the atmosphere, carrying with it magma fragments. Alternatively, high viscosity may slow ascent to where permeable outgassing through the vesicular and perhaps fractured magma results in lava effusion to produce domes and flows. In low viscosity magmas, typically basalts, bubbles may ascend buoyantly, allowing efficient magma outgassing and relatively quiescent magma effusion. Alternatively, bubbles may coalesce and accumulate to form meter-size gas slugs that rupture at the surface during strombolian eruptions. At fast magma

ascent rates, even in low viscosity magmas, melt and exsolved gas remain coupled allowing for rapid acceleration and hydrodynamic fragmentation in hawaiian eruptions.

4.1 Introduction

In the broadest sense, volcanic eruptions are either effusive or explosive. During explosive eruptions magma fragments and eruption intensity is ultimately related to the fragmentation mechanism and associated energy expenditure (Zimanowski *et al.* 2003). If the cause of fragmentation is the interaction of hot magma with external water, the ensuing eruption is called phreatomagmatic. Eruptions that do not involve external water are called “dry,” in which case the abundance and fate of magmatic volatiles, predominantly H₂O and CO₂, as well as magma rheology and eruption rate are the dominant controls on eruption style. Eruption styles are often correlated with magma composition and to some extent this relationship reflects differences in tectonic setting, which also influences magmatic volatile content and magma supply rate.

4.1.1 Getting magma to the surface

Volcanic eruptions represent the episodic or continuous surface discharge of magma from a storage region. We shall refer to this storage region as the magma chamber and to the pathway of magma ascent as the conduit. For magma to erupt, the chamber pressure has to exceed the sum of frictional and magma-static pressure losses, as well as losses associated with opening of the conduit. The latter may be due to tectonic forces and/or excess magma pressure, which in turn are a consequence of magma replenishment and/or volatile exsolution in a chamber within an elastically deforming wall rock. Magma-static pressure loss is strongly dependent on magma density, which is dependent on volatile exsolution and volume expansion as pressure decreases during ascent. Feedbacks between chamber and conduit can produce complex and unsteady eruptive behavior.

4.1.2 The volcanic conduit

Eruptions at basaltic volcanoes may begin as fissure eruptions, with typical dike widths of the order of one meter (Chapter 3; Wilson and Head 1981). However, magma often erupts at the surface through structures that more closely resemble cylindrical conduits. The processes by which flow paths become focused into discrete cylindrical vents are not well understood. One possibility is that the temperature-dependent viscosity of magma results in a feedback between a cooling, viscosity increase and reduction in flow velocity, so that the flow becomes more focused over time (Wylie-Lister 1995). In addition, thermal erosion may also contribute to flow focusing. (Bruce Huppert 1989).

The conduit during silicic explosive eruptions is generally thought to be more or less cylindrical, at least at shallow depths. However, the conduit cross-sectional area can change with depth and time because of wall-rock erosion, caused by abrasion as pyroclasts collide with conduit walls, or shear stress from the erupting magma, or wall collapse (Wilson *et al.* 1980, Macedonio *et al.* 1994, Kennedy *et al.* 2005, Mitchell 2005).

4.2 | Volatiles

Volatiles play the central role in governing the ascent and eruption of magma, as summarized in Figure 4.1. Dissolved volatiles, in particular water, have large effects on melt viscosity. Exsolved volatiles form bubbles of supercritical fluids, which we will also refer to as gas or vapor bubbles. These bubbles allow for significant magma compressibility and buoyancy, ultimately making eruption possible (Pyle and Pyle 1995, Woods and Cardoso 1997). The decrease in pressure associated with magma ascent reduces volatile solubility, leading to bubble nucleation and growth, the latter a consequence of both volatile exsolution and expansion (Sparks 1978). Volatile exsolution also promotes microlite crystallization, which in turn affects bubble growth and rheology – there is a complex feedback between decompression, exsolution, and crystallization (Tait *et al.*, 1989). The occurrence and dynamics of explosive eruptions are mediated by the initial volatile content of the magma, and the ability of gases to escape from the ascending magma.

4.2.1 Solubility

Volatile solubility is primarily pressure dependent, with secondary dependence on temperature, melt composition, and volatile speciation (McMillan 1994, Blank and Brooker 1994, Zhang *et al.*, 2007). Formulations for volatile solubility can be thermodynamic or empirical. In either case, calibration is achieved using measurements of dissolved volatile concentrations in quenched melts, equilibrated with a volatile phase of known composition at fixed pressures and temperatures. The principal species we consider here are H₂O and CO₂. Solubility of CO₂ in silicate melts is proportional to partial pressure, whereas for H₂O dissociation into molecular H₂O and OH results in a square root dependence on partial pressure. An empirical formulation for combined solubility of H₂O and CO₂ in rhyolitic melts at volcanologically relevant conditions is given by (Liu *et al.*, 2005)

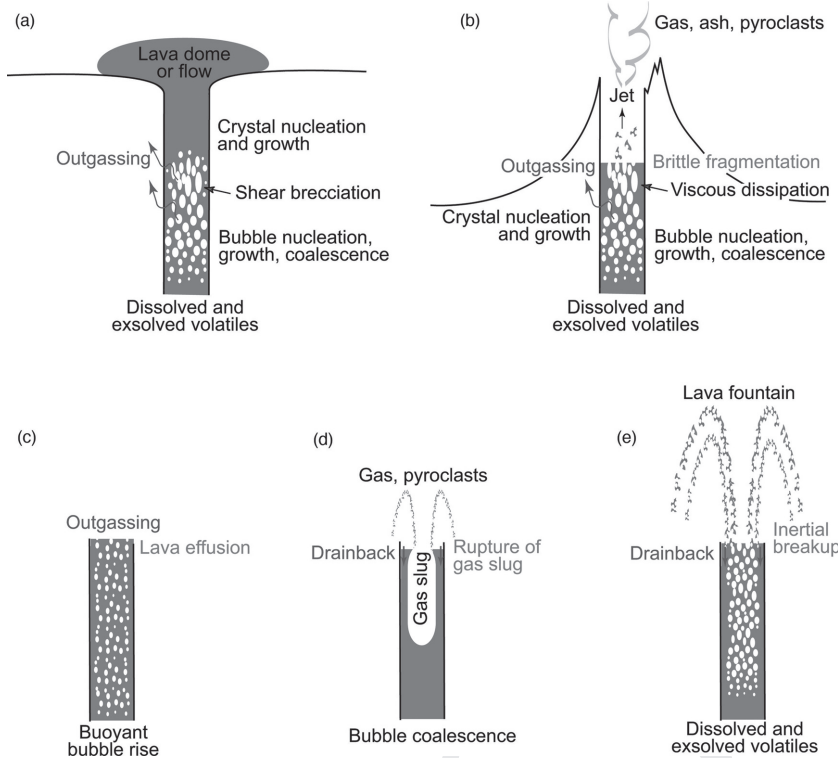


Figure 4.1 Schematic illustration of conduit processes.

(a) In effusive eruptions of silicic magma (high viscosity, low ascent rate) gas may be lost by permeable flow through porous and/or fractured magma. (b) During (sub)plinian eruptions bubble walls rupture catastrophically at the fragmentation surface and the released gas expands rapidly as the flow changes from a viscous melt with suspended bubbles to gas with suspended pyroclasts. (c) Extensive loss of buoyantly rising bubbles occurs during effusive eruptions of low-volatile content, low-viscosity magma. (d) Coalescence and accumulation of buoyant bubbles, followed by their rupture at the surface, produces strombolian explosions in slowly ascending low-viscosity magmas. (e) Bubbles remain coupled to the melt in low-viscosity, hawaiian eruptions, which are characterized by relatively high ascent rates, hydrodynamic fragmentation, and sustained lava fountaining.

$$C_w = 0.0012439 p_w^{3/2} + \frac{354.94\sqrt{p_w} + 9.623 p_w - 1.5223 p_w^{3/2}}{T} + p_c \left(-1.084 \times 10^{-4} \sqrt{p_w} - 1.362 \times 10^{-5} p_w \right) \quad (4.1)$$

and

$$C_c = p_c \left[\frac{5668 - 55.99 p_w}{T} + (0.4133\sqrt{p_w} + 0.002041 p_w^{3/2}) \right] \quad (4.2)$$

Here C_w is total dissolved H_2O in wt.%, C_c is dissolved CO_2 in ppm and T is temperature in Kelvin. p_w and p_c are the partial pressures in MPa of H_2O and CO_2 , respectively. This formulation is also approximately applicable to other melt compositions (Zhang *et al.*, 2007), but more accurate models are available (Dixon 1997, Newman and Lowenstern 2002, Papale *et al.*, 2006). Equilibrium concentrations of dissolved CO_2 and H_2O , based on this formulation, are shown in Figure 4.2. Notice that almost all CO_2 exsolves at >100 MPa for rhyolite and at >25 MPa for basalt, whereas most H_2O dissolves at <100 MPa for rhyolite and at <25 MPa for basalt. Consequently, processes in the shallow conduit are predominantly affected by H_2O exsolution.

4.2.2 Diffusivity

Volatile diffusivities in silicate melts are best characterized for H_2O . A recent formulation for

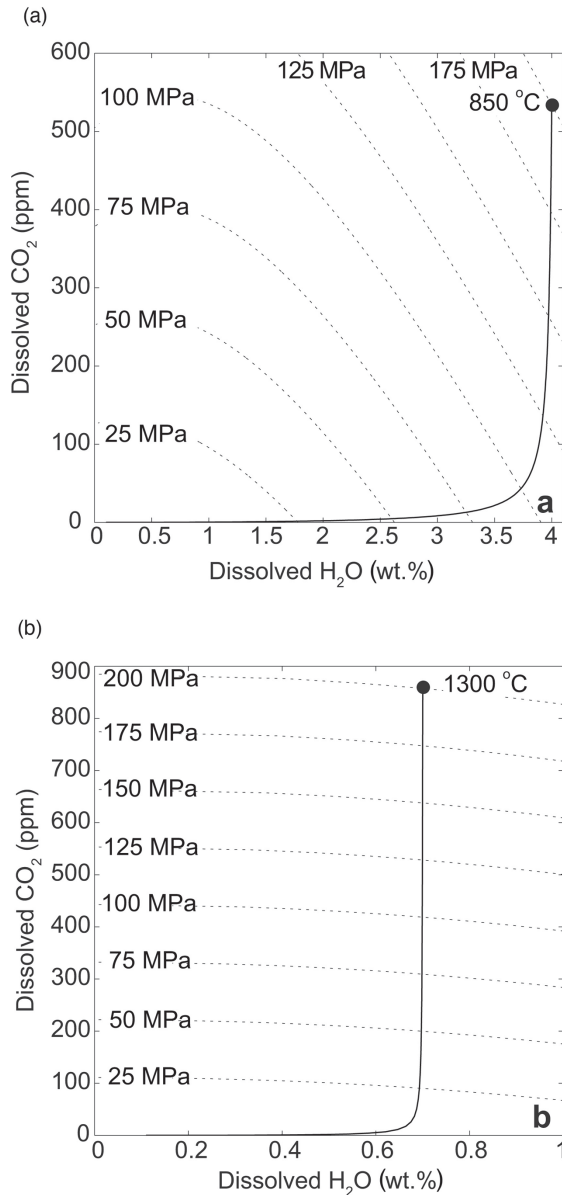


Figure 4.2 Solubility of CO₂ and H₂O (dashed contours) and equilibrium solubility degassing paths (solid lines) for typical rhyolitic and basaltic magmas undergoing closed-system degassing. (a) Rhyolite magma with no initial exsolved volatiles at 850 °C, initial pressure of 200 MPa, and initial dissolved H₂O content of 4 wt.%, using the solubility model of Liu *et al.* (2005). (b) Basaltic magma with no initial exsolved volatiles at 1300 °C, initial pressure of 200 MPa, and initial H₂O content of 0.7 wt.%, using the solubility model of Dixon (1997).

H₂O diffusivity (m² s⁻¹) in rhyolite with H₂O contents Σ 2 wt % is (Zhang and Behrens 2000)

$$D_{wr} = C_w \exp\left(-17.14 - \frac{10661}{T} - 1.772 \frac{p_m}{T}\right). \quad (4.3)$$

A formulation for higher H₂O concentrations is provided by Zhang *et al.* (2007), who also give the following equation for H₂O diffusivity in basalt

$$D_{wb} = C_w \exp\left(-8.56 - \frac{19110}{T}\right). \quad (4.4)$$

CO₂ diffusivity, D_c , is smaller than water diffusivity over a range of conditions (Watson 1994). The most reliable formulation for D_c in silicate melts is based on argon diffusivity, which is essentially identical to CO₂ at volcanologically relevant conditions (Behrens and Zhang 2001, Nowak *et al.*, 2004)

$$D_c = -18.239 - \frac{17367 + 1.0964 p_m}{T} + \frac{(855.2 + 0.2712 p_m) C_w}{T}.$$

4.2.3 Pre-eruptive volatile content of magmas

Water

Basaltic magmas show a wide range of water contents ranging from >0.5 wt.% to 6–8 wt.% (Johnson *et al.*, 1994, Wallace 2005), with non-arc basalts generally being considerably dryer than arc magmas, which have highly variable water contents. Silicic magmas also show a wide range of water contents up to 6 wt.%, and possibly higher (Carmichael 2002).

Carbon dioxide

CO₂ content of magmas is more difficult to constrain, because of its low solubility at shallow depths (Fig. 4.2). Measurements of H₂O and CO₂ in melt inclusions, in conjunction with solubility relations, suggest that arc magmas contain several wt.% of CO₂, much of which exsolved pre-eruptively, for example during vapor-saturated fractional crystallization (Papale 2005; Wallace 2005). Thus, arc magmas may already contain, or have lost, significant amounts of exsolved CO₂

prior to eruption. CO₂ of undegassed mid-ocean ridge basalts and ocean island basalts appears to be about 1 wt.% or less (Hauri 2002). Because CO₂ exsolves at greater pressures than H₂O, relative proportions of CO₂ and H₂O in erupted gases, glasses and, melt inclusions can provide constraints on depths of magma degassing. Because typical CO₂ contents of silicic magmas are considerably lower than H₂O, the latter dominates eruption dynamics.

Sulfur

H₂S and SO₂ are, after water and carbon dioxide, the most abundant magmatic volatiles. S concentrations are, at a minimum, several thousand ppm in arc and back-arc magmas (Wallace 2005). Volcanic sulfur emissions are spectrographically readily detectable and, therefore, play an important role in monitoring of active volcanoes via remote sensing. Emissions from active volcanoes, especially during voluminous explosive eruptions, have significant environmental and atmospheric impacts (Bluth *et al.*, 1993). Measured SO₂ fluxes from erupting volcanoes often exceed by one to two orders of magnitude the amounts thought to be dissolved in the magma prior to eruption. This “excess sulfur” problem is sometimes attributed to an exsolved S-bearing volatile phase accumulating within the magmatic system prior to eruption (Wallace *et al.*, 2003).

Chlorine and Fluorine

Measurable Cl and F are also present in volcanic gases, with Cl concentrations in the range of hundreds to thousands ppm in arc and back-arc magmas (Wallace 2005). Because S is less soluble than Cl, which in turn is less soluble than F (Carroll and Webster, 1994), these gases are also used to constrain depths of volatile exsolution and magma degassing histories (Allard *et al.*, 2005).

4.3 Bubbles

The “birth,” “life,” and “death” of bubbles are key to understanding the dynamics of volcanic eruptions and are the subject of this section.

4.3.1 Nucleation

Pressure decreases as magma ascends. If the concentration of dissolved volatiles exceeds the equilibrium solubility at a given pressure, the melt is supersaturated, a requirement for bubble nucleation. Supersaturation, ϵp_s , is defined as the difference between actual pressure and the pressure at which the concentration of dissolved volatiles would be in equilibrium with the co-existing vapor phase. The supersaturation required for nucleation corresponds to the energy that must be supplied to increase the surface area between two fluids. It is a consequence of surface tension, γ , a measure of the attractive molecular forces that produce a jump in pressure across a curved interface between two fluids. This so-called Laplace or capillary pressure is $2\gamma/R$ for a spherical bubble of radius R . Supersaturation is typically produced when fast magma ascent allows insufficient time for volatile diffusion into existing bubbles, which occurs when $\tau_{\text{diff}}/\tau_{\text{dec}} \gg 1$ (Toramaru, 1989). Here, $\tau_{\text{dec}} = p_m/\dot{p}_m$ is the characteristic decompression time, $\tau_{\text{diff}} = (S - R)^2/D$ is the characteristic time for volatile diffusion, S is the radial distance from bubble center to the midpoint between adjacent bubbles, D is volatile diffusivity in the melt, p_m is pressure of the melt, and \dot{p}_m is the decompression rate.

Bubble nucleation can be heterogeneous or homogeneous. In heterogeneous nucleation, crystals provide substrates that facilitate nucleation because of the lower interfacial energy between solid and vapor than between melt and vapor. Typically, ϵp_s is a few MPa for heterogeneous nucleation (Hurwitz and Navon, 1994, Gardner and Denis, 2004, Gardner, 2007) and ~10 to 100 MPa for homogeneous nucleation, in which nucleation sites are lacking (Mangan and Sisson, 2000).

Classical nucleation theory (Hirth *et al.*, 1970) predicts a very strong dependence of the nucleation rate J (number of bubbles per unit volume per unit time) on ϵp_s and γ

$$J \propto \exp\left[-\frac{16\pi\gamma^3\psi}{3k_b T \Delta p_s^2}\right]. \quad (4.5)$$

Here k_b is the Boltzmann constant and γ is typically 0.05 to 0.3 N m⁻¹, with a dependence on

both temperature and composition of the melt (Bagdassarov *et al.*, 2000, Mangan and Sisson, 2005). ψ is a geometrical factor that ranges between 0 and 1, depends on θ , the contact angle between bubble and crystal, and is given by

$$\psi = \frac{(2 - \cos\theta)(1 + \cos\theta)^2}{4}. \quad (4.6)$$

J determines the number density of bubbles per unit volume of melt, N_d and if bubbles nucleate at large $\mathcal{E}p_s$, they do so at a high rate.

4.3.2 Growth

As ambient pressure, p_m , decreases during magma ascent, bubbles may grow if volatiles exsolve and the vapor expands. The momentum balance for a growing bubble is obtained by neglecting inertial terms in the Rayleigh-Plesset Equation (Scriven, 1959). This is justified because large melt viscosities and short length scales result in Reynolds numbers for bubble growth $\ll 1$. The resulting equation for a bubble surrounded by a shell of melt with constant viscosity is (Proussevitch *et al.*, 1993)

$$p_g - p_m = \frac{2\gamma}{R} + 4\eta_0 v_r \left(\frac{1}{R} - \frac{R^2}{S^3} \right). \quad (4.7)$$

Here, p_g is the pressure inside the bubble, η_0 is the Newtonian melt viscosity, and v_r is the radial velocity of the melt-vapor interface, i.e., bubble wall. An idealized uniform packing geometry is assumed, so that each bubble can be represented as a sphere of radius R surrounded by a spherical melt shell of thickness $S - R$. In this formulation the time-dependent p_m couples bubble growth with magma ascent. Mass conservation of volatiles requires that

$$d(\rho_g R^3) = 4R^2 \rho_m \sum_i D_i \left(\frac{\partial C_i}{\partial r} \right)_{r=R} dt, \quad (4.8)$$

where r is radial distance from the center of the bubble, t is time, ρ_g is the pressure-dependent vapor density, ρ_m is melt density, D_i is the concentration dependent diffusivity of dissolved volatile species i , and C_i is the mass fraction of dissolved volatile i . Volatile diffusion is governed by

$$\frac{\partial C_i}{\partial t} + v_r \frac{\partial C_i}{\partial r} = \frac{1}{r^2} \frac{\partial C_i}{\partial r} \left(D_i r^2 \frac{\partial C_i}{\partial r} \right), \quad (4.9)$$

with v_r as the radial velocity of melt at radius r . The boundary condition at $r = S$ is $\partial C_i / \partial r = 0$. At $r = R$ the prescribed concentration is obtained from a suitable solubility model with the additional assumption that dissolved volatiles at the melt-vapor interface are locally in equilibrium with the vapor at p_g .

Under most conditions bubble growth is either limited by (1) the rate of viscous flow of the melt to accommodate the ensuing volume increase, (2) diffusion rate of volatiles to the melt-vapor interface where they can exsolve, or (3) the change in solubility caused by decompression. For each growth limit it is possible to simplify the solution of the governing equations or to derive analytical growth laws.

Modeling of bubble growth

Explicit modeling of diffusive bubble growth during magma ascent was first presented by Sparks (1978), based on the equations of Scriven (1959) and Rosner and Epstein (1972). Subsequently, Proussevitch *et al.* (1993) applied a model that included the diffusion of volatiles to bubble growth in magmas. This model was enhanced by Sahagian and Proussevitch (1996) and Proussevitch and Sahagian (1998) to include the thermal effects associated with the heat of volatile exsolution and the work done against the surrounding melt by bubble expansion. Figure 4.3 shows the results for the diffusive bubble growth in a rhyolite containing both H_2O and CO_2 .

Viscous limit

In the viscous limit $\tau_{vis}/\tau_{dec} \gg 1$ and bubble growth is retarded, following an exponential growth law (Lensky *et al.*, 2004). Here $\tau_{vis} = \eta_0/(p_g - p_m)$ is the characteristic viscous timescale. The viscous limit to bubble growth is the consequence of fast decompression rates relative to the viscous deformation of melt by the growing bubbles, and is most significant at melt viscosities in excess of 10^9 Pa s (Sparks *et al.*, 1994), which in the absence of significant

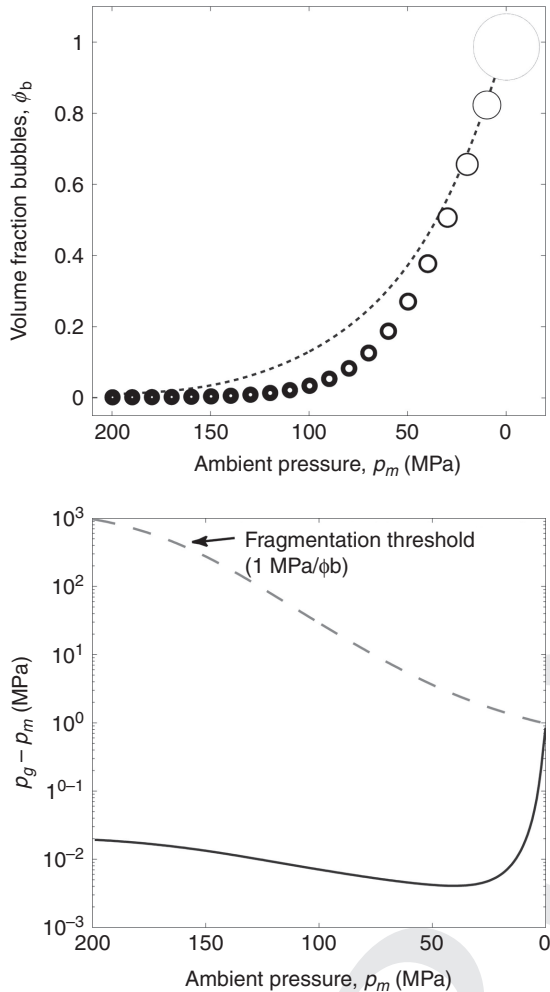


Figure 4.3 Model results for diffusive bubble growth in rhyolite with initial conditions of bubble volume fraction $\phi_0 = 0.001$, bubble number density $N_d = 10^{11} \text{ m}^{-3}$, 5 wt.% H_2O , 268 ppm CO_2 , $T = 850 \text{ }^\circ\text{C}$, magma pressure $p_m = 200 \text{ MPa}$, and decompression rate $\Delta p = 0.1 \text{ MPa s}^{-1}$. (a) Circles represent cross-sections through bubbles along the modeled trend of ϕ_b vs. p_m . For reference, the short-dashed black line represents the equilibrium closed-system degassing trend. Initially ϕ_b remains lower than equilibrium because volatile diffusion is slower than Δp , and bubble overpressure $p_g - p_m \approx 2\gamma/R$. As bubble radius R increases and bubble separation, $S - R$, decreases, diffusion starts to keep pace with decompression and ϕ_b approaches equilibrium values. (b) Bubble overpressure, $p_g - p_m$, vs. p_m (solid curve), with fragmentation threshold, Δp_f (dashed curve) of Spieler *et al.* (2004). At $p_m < 30 \text{ MPa}$, bubble growth becomes viscously limited, a consequence of H_2O exsolution and increasing melt viscosity. Consequently, magma pressure p_m decreases more rapidly than bubble vapor pressure p_g until the bubble overpressure reaches the fragmentation threshold pressure, i.e., $p_g - p_m = \Delta p_f$.

amounts of crystals, is achieved for silicic melts at shallow depths and low H_2O content. Because of retarded bubble growth, p_g decreases at a slower rate than p_m , resulting in the build-up of overpressure with $p_g - p_m \gg 2\gamma/R$ (Fig. 4.3). At the same time, a high p_g inhibits volatile exsolution, causing supersaturated conditions. This is referred to as “viscosity quench” (Thomas *et al.*, 1994) and increases the potential for accelerated bubble nucleation and/or growth.

Diffusive limit

During decompression, the volatile concentration at the melt-vapor interface, based on the assumption of local equilibrium, decreases. This creates a concentration gradient for volatiles to diffuse to this interface and exsolve. If $\tau_{\text{dec}} \ll \tau_{\text{diff}}$, volatile concentrations will remain close to equilibrium throughout the melt. On the other hand, if $\tau_{\text{diff}}/\tau_{\text{dec}} \gg 1$ (i.e., at high decompression rates) the melt becomes supersaturated, which is a necessary condition for bubble nucleation (Lensky *et al.*, 2004). Furthermore, in the diffusive limit, volatiles with different diffusivities may fractionate (Gonnermann and Manga, 2005b; Gonnermann and Mukhopadhyay, 2007).

Solubility limit

During solubility-limited growth, bubbles are close to mechanical and chemical equilibrium, that is, $\tau_{\text{diff}}/\tau_{\text{dec}} \ll 1$ and $\tau_{\text{vis}}/\tau_{\text{dec}} \ll 1$ (Lensky *et al.*, 2004) so that both overpressure and supersaturation are small. Dissolved volatiles are near their equilibrium concentrations throughout the melt and bubble radius R can be directly calculated from mass balance, equilibrium solubility, and an equation of state. Conditions favorable to solubility-limited bubble growth are low melt viscosity and/or low magma ascent rates.

4.3.3 Coalescence

Coalescence takes place when bubbles come into increasingly close proximity and the melt film between bubbles ruptures. This may be the consequence of (1) gravitational or capillary drainage of interstitial liquid (Proussevitch *et al.*, 1993b); (2) coalescence-induced coalescence, whereby the deformation of coalesced bubbles by capillary forces induces a flow field

that brings nearby bubbles into proximity (Martula *et al.*, 2000); (3) bubble growth leading to stretching and thinning of the liquid film that separates individual bubbles (Borrell and Leal, 2008); and (4) advection and collision of bubbles by buoyancy or by magma flow (Manga and Stone, 1994).

Gravitational and capillary film drainage, as well as bubble collisions are probably most important in low viscosity magmas. A positive feedback between bubble coalescence, which increases bubble size, and bubble mobility due to buoyancy is expected (Section 4.3.5). Whereas capillary drainage is dominant at bubble radii < 3 cm, gravitational drainage becomes dominant at radii > 3 cm (Proussevitch *et al.*, 1993). A characteristic velocity for capillary drainage can be obtained by balancing the capillary pressure gradient, γ/R^2 , with viscous resistance to flow, $\eta_0 v_f/R^2$, where v_f is the velocity in the film. Because the bubble-melt surface is assumed to be a free-slip surface, the characteristic length scale is the bubble radius R rather than film thickness. The resultant scaling $v_f \sim \gamma/\eta_0$ highlights the importance of melt viscosity. Whether and at what rate bubble collisions result in coalescence depends on the Weber number, $We = 2\rho v^2 R/\gamma$, where v is the velocity at which two bubbles approach one another.

In high viscosity magmas bubbles remain essentially “frozen” in the melt and coalescence is principally a consequence of bubble growth. In this case, coalescence appears to create a permeable network of bubbles due to relatively persistent holes in the ruptured melt films (Klug and Cashman, 1996). Because the interfacial tension between melt and crystals tends to be lower than between gas and crystals, coalescence in the presence of crystals is expected to occur at greater film thickness than in the absence of crystals (Proussevitch *et al.*, 1993b).

4.3.4 Breakup

The breakup of bubbles into several smaller bubbles originates with their deformation by some combination of viscous stresses and inertial forces. In silicic magmas, the bubble Reynolds number, $Re_b = \dot{\epsilon} R^2 \rho/\eta_0$, will always be small and inertia can be neglected. Here $\dot{\epsilon}$ is

the strain rate in the melt caused by buoyant rise of the bubble or by magma flow. For small Re_b , deformation scales with the Capillary number, $Ca = \eta_0 \dot{\epsilon} R/\gamma$, which characterizes the relative importance of viscous stresses that tend to deform bubbles, and surface tension stresses that act to keep bubbles spherical. If Ca exceeds some critical value, Ca_{cr} , bubble elongation by the flow becomes large enough that bubbles will break up. The value of the Ca_{cr} depends on the steadiness of the flow, melt viscosity, and flow type. For the viscosities of silicate melts, Ca_{cr} should range from ~ 1 to $> 10^3$. In both types of flows, bubbles will become highly elongated before breakup occurs. Capillary numbers will generally be large enough in conduits for large deformation and breakup to occur. However, to achieve large deformation also requires large strains which may be limited to the sides of conduits. It is thought that tube pumice is a manifestation of these conditions (Marti *et al.*, 1999).

In basaltic magmas, inertial forces can no longer be neglected once bubbles become larger than a few centimeters. In this limit, velocity differences across bubbles can lead to breakup. The relative importance of inertial forces and surface tension forces is characterized by We , based on the velocity difference across the melt that surrounds the bubble. For large Re_b , breakup occurs if We exceeds a critical value, We_{cr} , which implies that there might be a maximum stable bubble size (Hinze, 1955). Although the actual value of We_{cr} depends on the origin of the velocity differences, it is generally between 1 and 5 for a wide range of flow conditions.

4.3.5 Bubble mobility

Bubbles are buoyant and their rise speed depends on size, volume fraction, and viscosity. If buoyant bubble rise is much slower than magma ascent, bubbles are dispersed throughout the continuous melt phase and move passively with the flow. Such flows are called “dispersed” and in the asymptotic limit of infinitesimally small dispersed bubbles the flow is termed “homogeneous.” If the velocity of buoyant bubble rise is similar to or greater than magma ascent velocities, bubbles are decoupled from the liquid phase

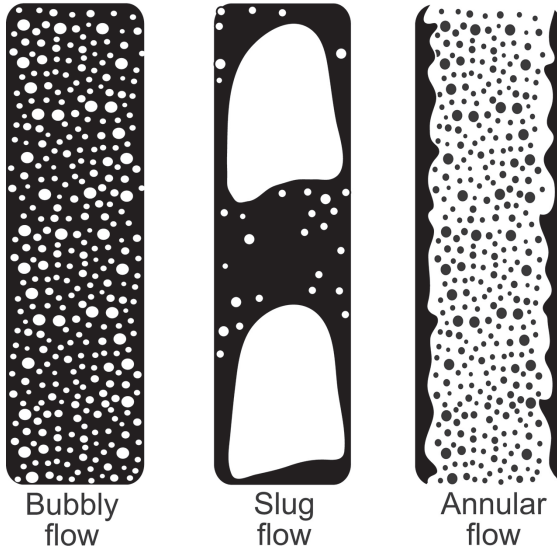


Figure 4.4 Flow regimes observed in bubble column experiments (e.g., Wallis, 1969). The gas phase is shown in white and the liquid phase in black.

and the flow is called “separated” (Brennen, 2005). During separated flow in laboratory experiments the topology of the gas and liquid phases is associated with different flow regimes (Fig. 4.4), that depend primarily on the relative volumetric flow rates of liquid and gas phase (Wallis, 1969). As this flux ratio increases to values of ~ 1 , the flow transitions from “bubbly flow,” where bubbles are randomly dispersed, to “slug flow,” where coalesced bubbles form rapidly ascending gas slugs of diameter comparable to the conduit diameter. At flux ratios above ~ 10 the flow transitions to “annular flow,” where the liquid phase forms an annular ring surrounding a cylindrical core of rapidly ascending gas. However, to what extent these different flow regimes are applicable to volcanic eruptions remains controversial (Chapter 6).

The terminal velocity of a single bubble containing vapor of viscosity η_g and density ρ_g , rising in an infinite liquid of viscosity η_0 and density ρ_m is (Batchelor, 1967)

$$U_t = \frac{R^2 g (\rho_m - \rho_g)}{3\eta_0} \frac{\eta_0 + \eta_g}{\eta_0 + \frac{3}{2}\eta_g}. \quad (4.10)$$

Therefore, bubbles within a silicic melt have negligible mobility, even at very low eruption rates, whereas significant bubble mobility can be expected for mafic melts. At finite volume fractions of bubbles, ϕ_b , hydrodynamic interactions reduce U_t by a factor $h(\phi_b)$, the hindering function. Various formulations exist for $h(\phi_b)$ and a commonly adopted one is the Richardson-Zaki equation (Richardson and Zaki, 1954)

$$h(\phi_b) = (1 - \phi_b)^n. \quad (4.11)$$

Here n is an empirical coefficient for the appropriate range of bubble size and flow conditions, typically with values around 2.5 (Zenit *et al.*, 2001). At flow regimes other than bubbly flow a different formulation for the relative velocity between gas and liquid phase has to be used (Dobran, 2001).

4.3.6 Bubbles and pressure loss

In general, mass discharge rate depends on the total pressure drop between magma chamber and vent. Within the conduit the pressure gradient is to first order the sum of magma-static pressure loss, $(dp/dz)_p$, and frictional pressure loss, $(dp/dz)_\eta$. Magma-static pressure depends on magma density and, hence, vesicularity as

$$\left(\frac{dp}{dz}\right)_p = \rho g \approx (1 - \phi_b) \rho_m g. \quad (4.12)$$

For dispersed bubbly flow the frictional pressure loss can be approximated on the basis of established single-phase flow correlations using the appropriate mixture viscosity (Ghiaasiaan, 2008)

$$\left(\frac{dp}{dz}\right)_\eta = \rho u^2 \frac{f}{a}, \quad (4.13)$$

where a is conduit radius, u is magma velocity, and f is the friction factor given by

$$f = \frac{16}{\text{Re}} + f_0. \quad (4.14)$$

Here $\text{Re} = 2u\rho a/\eta$, where η is the magma viscosity and f_0 has values of about 0.002–0.02 (Mastin

and Ghiorso, 2000). For highly viscous magmas the flow below the fragmentation level will, under most conditions, be laminar ($Re < 10^3$) and $f \propto 16/Re$. Above the fragmentation level the flow will be turbulent and $f \propto f_0$. For basaltic magma, frictional pressure loss over a wide range of ascent velocities is less than magma-static pressure loss and the flow dynamics will be more sensitive to changes in the density of the ascending magma than for eruptions where frictional pressure losses are larger. Consequently, under separated flow conditions there is potential for feedbacks between discharge rate, gas-to-melt flux ratios, and flow regime (Seyfried and Freundt, 2000; Guet and Ooms, 2006).

4.3.7 Permeable outgassing

The degassing history during ascent of an individual magma parcel may be complex and in many cases gas may separate from rising parcels of magma. We refer to this as outgassing, which may be a consequence of buoyant bubble rise, magma fragmentation, or permeable gas flow. Chapters 6 and 8 discuss outgassing associated with separated flow and high gas-to-melt flux ratios during strombolian and perhaps hawaiian eruptions. In some silicic eruptions high melt-to-gas flux ratios are also suggestive of decoupled gas flow (Edmonds *et al.*, 2003). However, high viscosities and negligible bubble mobility require that outgassing is associated with magma permeability, presumably a consequence of coalescing bubbles that form a permeable network (Eichelberger *et al.*, 1986; Klug and Cashman, 1996) and perhaps cracks and fractures produced by brittle magma deformation (Gonnermann and Manga, 2003; Gonnermann and Manga, 2005a; Tuffen *et al.*, 2003). It has been suggested that if conduit walls are permeable, which is controversial (Boudon *et al.*, 1998), then volatiles may also escape laterally from ascending magma into the conduit walls and permeable outgassing has the potential to modulate eruptive behavior (Jaupart and Allegre, 1991; Woods and Koyaguchi, 1994; Eichelberger, 1995).

Vesicularity-permeability measurements for volcanic rocks, and by inference magmas, are usually analyzed using the Kozeny-Carman

equation (Carman, 1956) where permeability, k , is given as

$$k(\phi_b) = \chi(\phi_b - \phi_{bp})^\beta. \quad (4.15)$$

Here χ is an empirical constant and ϕ_{bp} is the volume fraction of bubbles that corresponds to percolation threshold (Saar and Manga, 1999), with typical values of $2 \leq \beta \leq 4$. An uncontroversial permeability model for vesicular magma remains elusive (Takeuchi *et al.*, 2005; Wright *et al.*, 2009). Furthermore, it appears that the nature of magma deformation plays a critical role in creating permeability (Okumura *et al.*, 2008; Okumura *et al.*, 2010).

Permeable outgassing can be modeled as flow through a porous medium by combining the continuity equation for the exsolved volatile phase with Darcy's equation or, if the velocity of the gas phase becomes too large for inertial effects to be neglected, Forcheimer's equation (Rust and Cashman, 2004).

4.4 Crystal nucleation and growth

Crystals nucleate due to undercooling, which is predominantly a consequence of H_2O exsolution. Nucleation rates determine the crystal number density and size distribution, which provide a record of the magma's ascent history. During crystallization the volatile content of the residual melt phase increases because volatiles preferentially partition into the melt phase. This in turn affects bubble nucleation and growth, as well as melt viscosity.

Undercooling, the thermodynamic driving force for crystallization, is the chemical potential of H_2O in the melt and can be expressed as ϵT_i , the difference between actual temperature, T , and the liquidus temperature, T_i . Because the latter depends on composition and volatile content, bubble nucleation and growth will increase T_i and can result in sufficient undercooling for crystallization (Hammer, 2004). The rate of homogeneous nucleation of critical nuclei, I ($m^{-3} s^{-1}$), is given by classical nucleation theory as

$$I = I_0 \exp\left(-\frac{\Delta G^* + \Delta G_D}{k_B T}\right). \quad (4.16)$$

Here I_0 is a reference nucleation rate, k_B is the Boltzmann constant, and ΔG_D is the activation energy for diffusion (James, 1985). ΔG^* is the free energy required to form a spherical nucleus of critical size and depends on the free energy, σ , associated with the crystal-liquid interface. Therefore σ , nucleation rate increases with decreasing σ (Mueller *et al.*, 2000). The rate of heterogeneous nucleation also follows Eq. (4.16), but with a modified σ to account for the lower interfacial energies (Spohn *et al.*, 1988). Because σ is relatively poorly constrained, estimates of crystal nucleation rates are typically associated with large uncertainties. Moreover, the validity of classical nucleation theory and its assumptions that (1) the interface between nucleus and melt is sharp; (2) the critical nucleus has the thermodynamic properties of the bulk solid; and (3) σ can be treated as a macroscopic property equal to the value for a planar interface, remain controversial.

Once a crystal nucleates its growth rate, Y , is given by (Spohn *et al.*, 1988)

$$Y = Y_0 \left[1 - \exp\left(-\frac{\Delta H \Delta T_c}{k_B T_l T}\right) \right] \exp\left(-\frac{\Delta G_D}{k_B T}\right), \quad (4.17)$$

where Y_0 is a reference growth rate and ΔH is the change in enthalpy between melt and crystalline phases. If empirical parameters such as T_l and σ are known, the above equations can be used to model magma crystallization. Alternatively, parameterizations for I and Y can be used to explore the dependence of eruption behavior on syneruptive crystallization (Melnik and Sparks, 1999). The prediction of crystal size distributions is possible through the use of the Avrami equation (Marsh, 1998)

$$\phi_x = 1 - \exp(-k_v Y^3 t^4 I). \quad (4.18)$$

Here a given crystal volume fraction, ϕ_x , is assumed to correspond to thermodynamic equilibrium after crystallization over time, t , and with k_v as a volumetric factor.

4.5 | Magma rheology

Silicate melts form a disordered network of interconnected SiO_4 tetrahedra where the self-diffusive motion of atoms, called structural relaxation, results in a continuous unstructured rearrangement of the molecular structure. In the presence of an applied stress, this molecular rearrangement results in a directional motion of SiO_4 tetrahedra relative to one another and macroscopically manifests itself as viscous flow (Moynihan, 1995).

The intrinsic viscosity of silicate melts varies over orders of magnitude, even within a single volcanic eruption. It depends on the degree of polymerization, a function of chemical composition and volatile content. Within realistic ranges of compositional variability, eruptive temperature, and volatile content, the viscosity of basaltic melts may vary between about 10 and 10^3 Pa s, and between about 10^4 and 10^{12} Pa s or more for silicic melts (Fig. 4.5). Changes in viscosity during individual eruptions are especially pronounced at low pressures (depths <1 km), where most of the H_2O exsolves (Figs. 4.2 and 4.6). Magma rheology is discussed further in the context of lava flow emplacement in Chapter 5.

4.5.1 The effect of dissolved volatiles and temperature

Dissolved water dissociates into molecular water and hydroxyl ions, thereby depolymerizing the melt. In rhyolitic melts the effect of water content can be tremendous and exceeds the effect of temperature (Fig. 4.5), but it is less pronounced for mafic magmas (Giordano and Dingwell, 2003). In contrast, viscosity is less affected by CO_2 (Bourgue and Richet, 2001). Recent viscosity formulations applicable over a range of compositions, temperature, and water contents are discussed in Hui and Zhang (2007), Zhang *et al.* (2007), and Giordano *et al.* (2008).

4.5.2 The effect of deformation rate

If the applied rate of deformation exceeds a certain threshold, the induced molecular motions of the melt are no longer compensated by random reordering of the melt structure. This is

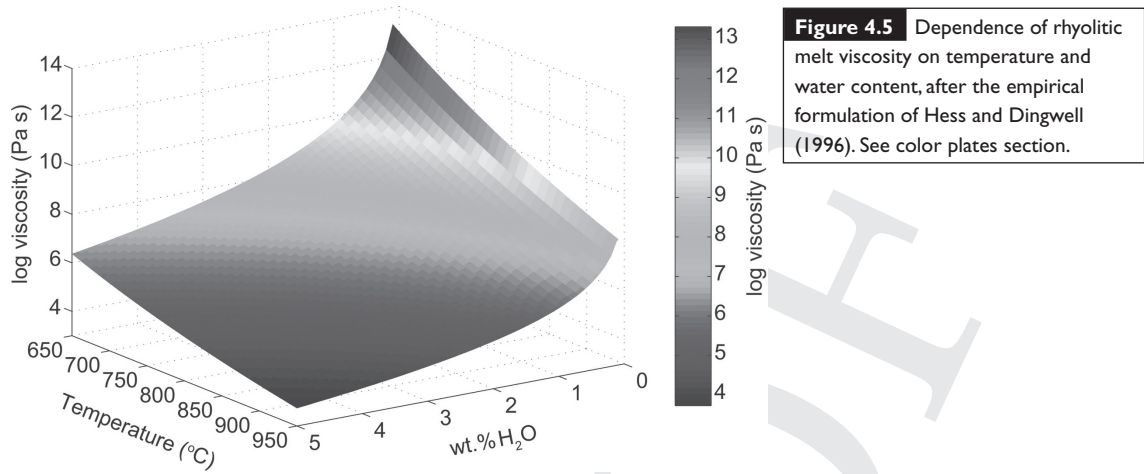


Figure 4.5 Dependence of rhyolitic melt viscosity on temperature and water content, after the empirical formulation of Hess and Dingwell (1996). See color plates section.

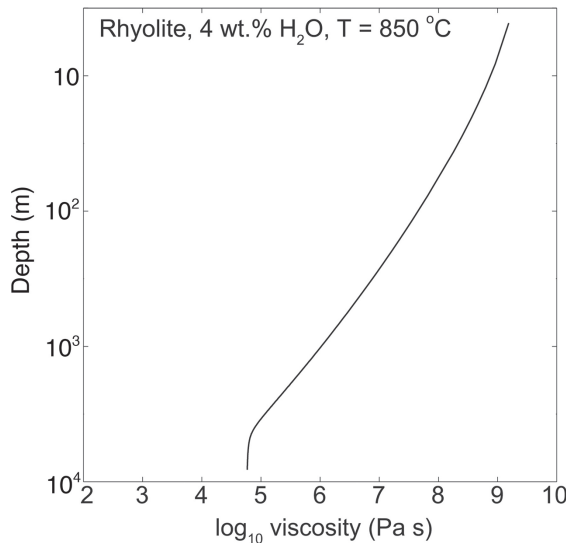


Figure 4.6 Dependence of rhyolitic melt viscosity (Hess and Dingwell, 1996) on depth, assuming lithostatic pressure and equilibrium volatile solubility. Note the wide range in viscosity and the tremendous viscosity increase at shallow depths, due to the exsolution of H₂O.

manifested in shear thinning, a decrease in viscosity from its “relaxed” or Newtonian value and will result in brittle failure if deformation rates exceed the onset of shear-thinning by approximately two orders of magnitude (Webb, 1997, and references therein). The strain rate at which shear thinning is first observed can be defined in terms of the viscous relaxation time, $\tau_r = \eta_0/G_\infty$, as

$$\dot{\epsilon}_{st} \sim 10^{-3} \frac{G_\infty}{\eta_0} \tag{4.19}$$

Here $G_\infty \sim 10^{10}$ Pa is the shear modulus and η_0 is the Newtonian melt viscosity, measured at $\dot{\epsilon} \ll \dot{\epsilon}_{st}$.

4.5.3 The effect of crystals

Crystals increase magma viscosity (Lejeune and Richet, 1995; Stevenson *et al.*, 1996; Arbaret *et al.*, 2007; Caricchi *et al.*, 2007; Lavallee *et al.*, 2007). For small crystal volume fractions, $\phi_x < 10 - 30\%$, and low strain rates, the viscosity of the crystalline magma relative to the crystal-free melt, $\eta_r = \eta/\eta_0$, can be approximated as

$$\eta_r = (1 - \phi_x/\phi_{xcr})^\alpha \tag{4.20}$$

Here ϕ_{xcr} represents a critical volume fraction at which crystals start to impede the ability of the suspension to flow and $\alpha \approx -2.5$ (Llewellyn and Manga, 2005). At ϕ_x greater than some value, typically in the range of 10–50%, crystals may come into contact creating a framework that provides a finite yield strength. Shear thinning and shear localization may occur as melt and crystals redistribute themselves to decrease the flow disturbance. It most likely occurs in a narrow zone near the conduit wall and may produce a plug flow that can manifest itself at the surface as volcanic spine. A viscosity formulation that is calibrated to a broad range of crystal

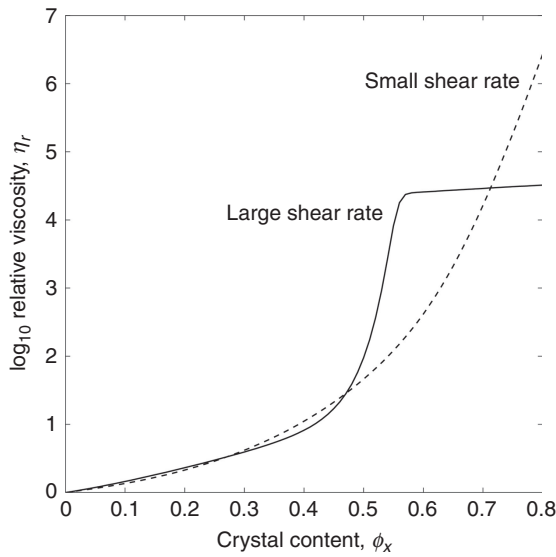


Figure 4.7 The effect of crystals on the relative mixture viscosity ($\eta_r = \eta/\eta_0$), based on Eq. (4.20), with parameters $\phi_{bcr} = -0.066499 \tanh(0.913424 \log(\dot{\epsilon}) + 3.850623) + 0.591806$; $\delta = -6.301095 \tanh(0.818496 \log(\dot{\epsilon}) + 2.86) + 7.462605$; $\alpha = -0.000378 \tanh(1.148101 \log(\dot{\epsilon}) + 3.92) + 0.999572$; $\beta = 3.987815 \tanh(0.8908 \log(\dot{\epsilon}) + 3.24) + 5.099645$.

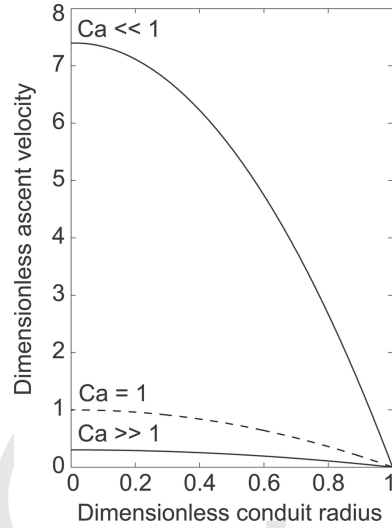


Figure 4.8 The effect of bubbles at small and large Ca on the velocity profile in a cylindrical conduit for a given pressure gradient. Dashed curve is the bubble-free reference case $Ca = 1$ (or equivalently $\phi_b = 0$). Both solid curves are for $\phi_b = 0.6$ and $\phi_{bcr} = 0.75$ in Eq. (4.21).

content and strain rates (Fig. 4.7) is provided by Caricchi *et al.* (2007)

$$\eta = \eta_0 \left[1 + \left(\frac{\phi_x}{\phi_{xcr}} \right)^\delta \right] \left[1 - \alpha \operatorname{erf} \left(\frac{\sqrt{\pi}}{2\alpha} \frac{\phi_x}{\phi_{xcr}} \left[1 + \left(\frac{\phi_x}{\phi_{xcr}} \right)^\beta \right] \right) \right]^{-B\phi_{xcr}} \quad (4.21)$$

Here $B = 2.5$ and the remaining empirical parameters δ , α , and β are provided in Figure 4.7.

4.5.4 The effect of bubbles

The effect of bubbles on viscosity depends on whether the bubbles are able to deform and is a function of $Ca = \eta_0 \dot{\epsilon} R / \gamma$. If $Ca \ll 1$, bubbles remain nearly spherical and the viscosity is greater than that of the melt (Taylor, 1932). In contrast, for $Ca > 0(1)$, bubbles can become elongated (Rust *et al.*, 2003) and the viscosity decreases (Chapter 5; Bagdassarov and Dingwell, 1992; Manga *et al.*, 1998; Lejeune *et al.*

1999; Stein and Spera, 2002). An expression for this dependence on Ca is given by Pal (2003) as

$$\eta_r \left(\frac{1 - 12\eta_r^2 Ca^2 / 5}{1 - 12Ca^2 / 5} \right)^{-4/5} = \left(1 - \frac{\phi_b}{\phi_{bcr}} \right)^{-\phi_{bcr}} \quad (4.22)$$

where ϕ_{bcr} is an empirical parameter that is conceptually analogous to ϕ_{xcr} . The strain-rate dependent rheology of melt with suspended bubbles and crystals is derived from a linear superposition of the individual dependencies (Thies, 2002). As illustrated in Figure 4.8, during laminar flow at a given pressure gradient, the presence of bubbles can increase or decrease mass discharge rate by almost one order of magnitude. Chapter 5 further considers the combined effects of bubbles and crystals on magma rheology (Section 5.2.2).

4.6 Magma fragmentation

During all explosive eruptions pyroclasts are ejected from the volcanic vent. Here we focus on “dry” magma fragmentation, which does

not involve any interaction with non-magmatic water. The type and efficiency of the fragmentation process determines pyroclast size and how much magmatic gas is released per unit mass of magma. This, in turn, has implications for the volcanic jet, column, and plume that are produced when the gas-pyroclast mixture exits the volcanic vent (Chapters 8 and 9). Fragmentation is thought to occur when specific conditions are reached within the conduit. The proposed criteria for fragmentation include: (1) a critical bubble volume fraction; (2) a stress criterion; (3) a strain-rate criterion; (4) a potential energy criterion; and (5) an inertial criterion.

The critical volume fraction criterion is thought to arise from some form of instability within the thin bubble walls, once $\phi_b \approx 0.75$ is reached (Verhoogen, 1951; Sparks, 1978). However, magma fragments have vesicularities that range from 0 (obsidian) to >98% (reticulite) implying that a fragmentation criterion governed by a critical volume fraction cannot be generally applicable (though very high vesicularities may reflect post-fragmentation growth of bubbles).

The stress criterion is based on the view that fragmentation in high-viscosity magmas takes place when volatile overpressure, ϵp_f , exceeds the tensile strength of the melt and ruptures bubble walls (Alidibirov, 1994; Zhang, 1999). Spieler *et al.* (2004) provide a formulation with good fit to a broad range of experimental data

$$\Delta p_f = 10^6 \text{ Pa} / \phi_b, \quad (4.23)$$

that has been modified by Mueller *et al.* (2008) to account for permeable gas flow.

The strain-rate criterion is based on the observation that silicate melts can fragment if deformation rates exceed the structural relaxation rate of the melt at $\dot{\epsilon} \sim 10^2 \dot{\epsilon}_{st}$ (Section 4.5.2). It is thought to be the consequence of a rapid decompression that forces rapid bubble growth (Papale, 1999). Ittai *et al.* (2010) have argued that both the stress criterion and the strain-rate criterion are equivalent, because of their mutual dependency on shear modulus and magma rheology.

Namiki and Manga (2005) suggested a potential energy criterion, based on the observation that during rapid decompression ϕ_b and ϵp_f determine the expansion velocity of a bubbly liquid. Potential energy depends on both ϕ_b and ϵp_f (Mastin, 1995), with fragmentation taking place above some threshold.

Hydrodynamic or inertial fragmentation should be predominantly associated with mafic magma, where rapid decompression results in rapid bubble growth, inertial stretching, and hydrodynamic breakup (Shimozuru, 1994; Zimanowski *et al.*, 1997; Villermaux, 2007). A criterion for inertial fragmentation is based on the Reynolds number, Re_v , and Weber number, We_v , of the expanding magma (Namiki and Manga, 2008)

$$Re_v = \frac{\rho(1-\phi_b)v^2L}{3\eta_0} > O(1) \quad (4.24)$$

and

$$We_v = \frac{\rho(1-\phi_b)v^2L}{\gamma} \gg 1. \quad (4.25)$$

Here L is a characteristic length scale and v is the expansion velocity of the vesicular magma, which can be obtained from the bubble growth rate.

4.7 | Modeling of magma ascent

The past decade has seen much progress in modeling magma ascent (Sahagian, 2005). In contrast to the modeling of effusive eruptions, explosive eruptions require a criterion to estimate the depth of magma fragmentation, and merging of a model for the bubbly flow region below the fragmentation level with one for the gas-pyroclast region above. Flow in the gas-pyroclast flow region is compressible and is typically modeled as one-dimensional with a parameterization for wall friction and granular stresses during highly turbulent flow (Wilson and Head, 1981; Dobran, 1992; Koyaguchi, 2005).

Conduit models may be steady or time-dependent. The steady approximation is

reasonable when the timescales over which changes in eruption rate and geometry exceed ascent times (Slezin, 2003). Time-dependent behavior becomes important when ascent times are similar to the timescale over which boundary conditions change. This can be a consequence of coupling between magma flow and (1) magma storage; (2) conduit wall elasticity; (3) magma compressibility; (4) magma outgassing; (5) viscous dissipation; and (6) magma rheology. A departure from one-dimensional models is necessary if lateral variations in properties are important, for example due to shear-rate dependent viscosity, shear localization, viscous dissipation, or permeable outgassing into conduit walls.

Dispersed two-phase flow below the fragmentation level is typically treated as homogeneous, using an appropriate magma viscosity. Above the fragmentation level, the homogenous flow assumption is sufficient if fragments are $\sum 10^{-4}$ m in diameter (Papale, 2001). However, treating the flow as separated for larger fragments results in a more accurate characterization of ascent velocity (Dufek and Bergantz, 2005). In the case of separated flow above or below the fragmentation level there are two classes of models, those that explicitly incorporate interfacial momentum exchanges and those that do not (Dobran, 2001). Separated flow models with no interfacial momentum exchange treat the flow as single-phase, but incorporate closure laws for the gas volume fraction and frictional pressure loss of the two-phase mixture (Wilson and Head, 1981). Separated models with interface exchange allow for different gas and liquid (pyroclast) velocities and flow directions. However, a priori assumptions about the flow regime are required for these closure laws.

4.7.1 Steady homogeneous flow in one dimension

Below the fragmentation level homogeneous flow models advect bubbles passively with the melt. That is $U_t \ll U_m$ and $u = U_m = U_b$, where U_b is the bubble velocity. Together with the assumption of constant mass flux throughout the conduit, Q , the equation of mass conservation becomes

$$\frac{dQ}{dz} = \frac{d}{dz}(\rho u A) = 0. \quad (4.26)$$

Here A is conduit cross-sectional area and ρ is the bulk density of bubbly magma, given by $\phi_b \rho_g + (1 - \phi_b) \rho_m$. The value of ρ_g may be obtained from the ideal gas law, but use of another equation of state may be more appropriate at high pressures (Kerrick and Jacobs, 1981). ρ_m can be obtained from empirical formulations (Lange, 1994), but in many cases the melt phase is assumed to be incompressible. The bubble volume fraction ϕ_b depends on ρ_g and the amount of exsolved volatiles. If it is assumed that bubble growth is limited by solubility, the amount of exsolved volatiles per unit mass of melt is equal to the initial volatile concentration minus the equilibrium solubility at the given pressure. However, in many eruptions bubble growth is viscously and/or diffusively limited, requiring a concurrent calculation for bubble growth. If permeable outgassing is important, Eq. (4.26) may include a sink term based on a suitable porosity-permeability relation and Darcy's law or Forcheimer's equation for radial gas flow to the conduit walls and/or upward gas flow to the vent (Jaupart and Allegre, 1991).

Equation (4.26) states that mass flux is constant and volume expansion of the magma by bubble growth must be balanced by acceleration and/or by an increase in conduit cross-sectional area. Assuming a vertical conduit of cylindrical shape, conservation of momentum is governed by (Mastin and Ghiorso, 2000; Dobran, 2001)

$$\rho u \frac{du}{dz} = -\frac{dp}{dz} - \left(\frac{dp}{dz}\right)_p - \left(\frac{dp}{dz}\right)_\eta = -\frac{dp}{dz} - \rho g - \rho u^2 \frac{f}{a}. \quad (4.27)$$

Expanding Eq. (4.26) and substituting for du/dz in Eq. (4.27) gives

$$-\frac{dp}{dz} = \rho g + \rho u^2 \frac{f}{a} - \frac{\rho u^2}{A} \frac{dA}{dz} - u^2 \frac{d\rho}{dz}. \quad (4.28)$$

Equation (4.28) indicates that the change in magma pressure with respect to height depends, from left to right, on magma-static

pressure loss, frictional pressure loss, change in conduit diameter, and change in magma density. Assuming isentropic conditions (denoted by subscript S), that is an infinitesimal reversible pressure change and negligible time for heat transfer, then

$$\frac{d\rho}{dz} = \left(\frac{\partial\rho}{\partial p}\right)_S \frac{dp}{dz} = \frac{1}{c^2} \frac{dp}{dz}. \quad (4.29)$$

Here c is the speed of sound in the magma and using the Mach number, $M = u^2/c^2$, Eq. (4.28) becomes

$$-\frac{dp}{dz}(1-M^2) = \rho g + \rho u^2 \frac{f}{a} - \frac{\rho u^2}{A} \frac{dA}{dz}. \quad (4.30)$$

Equations (4.26) and (4.30) are applicable to homogeneous flow above or below the fragmentation level and can be solved with standard numerical methods (Press *et al.*, 1992). There are two solution approaches: (1) set dp/dz to be constant, for example lithostatic, and then dA/dz and u can be calculated, or (2) if A is known, then conduit entrance and exit pressures are specified and dp/dz and u can be calculated (Wilson and Head, 1981; Giberti and Wilson, 1990; Dobran, 1992; Mastin and Ghiorso, 2000). For $M < 0.3$ the effect of magma compressibility on the flow can be neglected, whereas for $M > 0.3$ magma compressibility contributes to the change in pressure of the ascending magma. If $p = 1$ atm at the vent exit, then the right-hand side of Eq. (4.28) has to go to zero to avoid a singular solution as M approaches 1. Therefore, the conduit flares upward with

$$\frac{da}{dz} = \frac{1}{2} \left(\frac{g a}{u^2} + f \right) > 0. \quad (4.31)$$

This result can be derived by setting the right-hand side of Eq. (4.28) to zero with $A = \pi a^2$ (Mastin and Ghiorso, 2000). If Eq. (4.31) is satisfied at $M < 1$ and the conduit above continues to flare, the magma will decelerate. On the other hand if $M = 1$, the magma will accelerate to supersonic velocities and p will continue to decrease, potentially to values below 1 atm. If that is the case, a shock wave will

adjust the flow back to 1 atm at the vent exit. If the exit pressure exceeds 1 atm, the flow is “choked,” that is $M = 1$ and the exit velocity is equal to c , the speed of sound in the gas-pyroclast mixture.

In many cases the assumption of isothermal conditions is reasonable; if not, an equation for conservation of energy has to be added (Mastin and Ghiorso, 2000; Dobran, 2001)

$$dH + udu + gdz = 0. \quad (4.32)$$

Here H is the specific enthalpy of the melt-gas mixture from which the magma temperature can be calculated.

4.7.2 Steady separated flow in one dimension

As discussed in Section 4.3.5, the flow of the separated melt and gas phases below the fragmentation level may occur under different regimes. Criteria that determine the transitions between individual flow regimes, as well as formulations for interphase drag forces, F_{mg} , need to be specified. Existing models do not predict the occurrence of flow-regime transitions, but rather rely on a-priori assumptions about the occurrence of flow transitions, equivalent to the flow transition associated with magma fragmentation. For example, the model of Dobran (1992) is based on the assumption of a constant mass flow rate through the conduit

$$\frac{d}{dz} (Q_g + Q_{gd}) = 0 \quad (4.33)$$

and

$$\frac{d}{dz} (Q_m - Q_{gd}) = 0. \quad (4.34)$$

Here subscript g denotes the exsolved volatile phase, gd the dissolved volatile phase, and m the melt phase. As in the homogeneous flow model it is possible to account for permeable gas loss through an additional flux term on the right-hand side of Eq. (4.36). The momentum equations for the exsolved volatile and the melt phases are, respectively

$$\rho_g u_g \phi_b \frac{du_g}{dz} = -\phi_b \frac{dp}{dz} - F_{mg} - F_{wg} - \rho \phi_b g \quad (4.35)$$

and

$$\rho_m u_m (1 - \phi_b) \frac{du_m}{dz} = -(1 - \phi_b) \frac{dp}{dz} - F_{mg} - F_{wm} - \rho_m (1 - \phi_b) g. \quad (4.36)$$

Here F_{wg} and F_{wm} are the wall drag forces for the phase that is assumed to be in contact with the conduit wall. For example, Dobran (1992) used $F_{wm} = (dp/dz)_\eta$, $F_{wg} = 0$ below the fragmentation level and $F_{wm} = 0$, $F_{wg} = (dp/dz)_\eta$ above.

4.7.3 Two-dimensional flow

If magma flow is radially non-uniform, a two-dimensional modeling approach can provide additional insight. Cases where two-dimensional modeling has been important involve non-Newtonian magma rheology and shear heating, as well as permeable outgassing and heat loss through the conduit walls.

The direct approach is to solve the Navier-Stokes equations in two cartesian or axisymmetric cylindrical coordinates. For axisymmetric homogeneous flow, conservation of momentum is given by (Bird *et al.*, 1960)

$$\begin{aligned} \rho \frac{\partial u_r}{\partial t} + \rho u_r \frac{\partial u_r}{\partial r} + \rho u_z \frac{\partial u_r}{\partial z} \\ = -\frac{\partial p}{\partial r} - \frac{1}{r} \frac{\partial}{\partial r} (r \tau_{rr}) - \frac{\tau_{rz}}{z} \end{aligned} \quad (4.37)$$

and

$$\begin{aligned} \rho \frac{\partial u_z}{\partial t} + \rho u_r \frac{\partial u_z}{\partial r} + \rho u_z \frac{\partial u_z}{\partial z} \\ = -\rho g - \frac{\partial p}{\partial z} - \frac{1}{r} \frac{\partial}{\partial r} (r \tau_{rz}) - \frac{\partial \tau_{zz}}{\partial z}, \end{aligned} \quad (4.38)$$

with stress tensors

$$\tau_{rr} = -2\eta \frac{\partial u_r}{\partial r} - \lambda \left(\frac{1}{r} \frac{\partial}{\partial r} (r u_r) + \frac{\partial u_z}{\partial z} \right), \quad (4.39)$$

$$\tau_{zz} = -2\eta \frac{\partial u_z}{\partial z} - \lambda \left(\frac{1}{r} \frac{\partial}{\partial r} (r u_r) + \frac{\partial u_z}{\partial z} \right), \quad (4.40)$$

and

$$\tau_{rz} = -\eta \left(\frac{\partial u_z}{\partial r} + \frac{\partial u_r}{\partial z} \right). \quad (4.41)$$

Here $\lambda = \frac{2}{3} \eta - K$, where η is the viscosity of the magma. K is called the bulk viscosity, which accounts for the compressibility of the two-phase magma mixture (Massol *et al.*, 2001) and is often assumed negligible. Various simplifications of Eqs. (4.37) and (4.38) can be employed. If the flow is laminar ($Re < 10^3$), which is usually the case below the fragmentation level, the second and third terms on the left-hand side can be neglected. Furthermore, if the flow is steady the time derivatives are zero. Assuming isothermal conditions, the momentum equations are complemented by an equation for the conservation of mass

$$\frac{\partial \rho}{\partial t} + \frac{1}{r} \frac{\partial}{\partial r} (\rho r u_r) + \frac{\partial}{\partial z} (\rho u_z) = 0. \quad (4.42)$$

Examples of recent two-dimensional conduit models are given by Collier and Neuberg (2006); Costa *et al.* (2007a,b); Hale (2007); Hale and Muehlhaus (2007).

If vertical flow is a reasonable approximation ($u = u_z$, $u_r = 0$), Eqs. (4.37) and (4.38) become

$$\frac{\partial}{\partial r} (r \tau_{rz}) = -r \frac{\partial p}{\partial z}, \quad (4.43)$$

and upon integration

$$\tau_{rz} = -\eta \frac{\partial u_z}{\partial r} = -\frac{r}{2} \frac{\partial p}{\partial z}. \quad (4.44)$$

The relative ease with which Eq. (4.44) can be solved makes it easier to model more complex magma rheologies (Costa and Macedonio, 2005; Mastin, 2005; Vedeneva *et al.*, 2005), and to include subgrid scale calculations of bubble growth, where the model for bubble growth is discretized at a smaller scale than the conduit model itself (Fig. 4.9; Gonnermann and Manga, 2003, 2007).

To investigate the role of shear heating or magma cooling near the conduit walls, an energy equation has to be included. Neglecting thermal diffusion in the vertical direction, the energy equation is (Bird *et al.*, 1960)

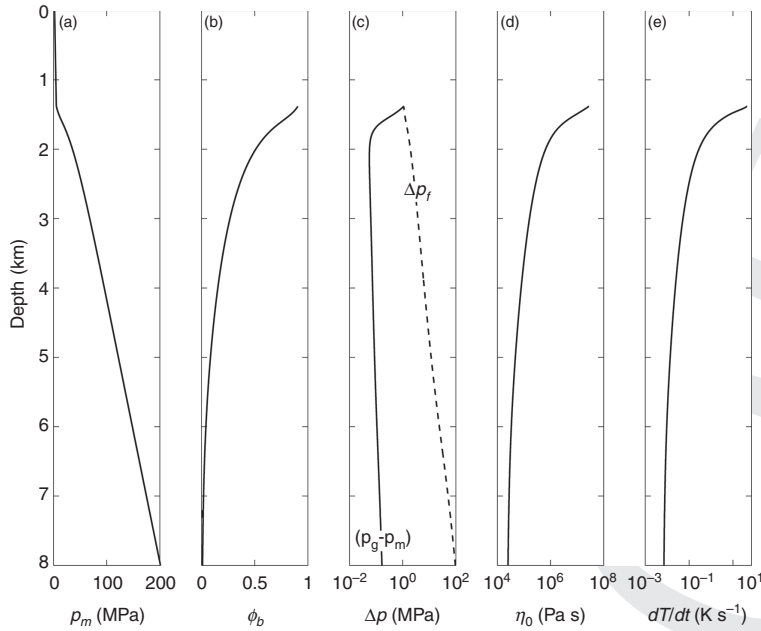


Figure 4.9 Illustrative model for rhyolite magma rising in a cylindrical conduit of 30 m diameter using Eq. (4.43) with sub-grid scale diffusive bubble growth at a constant bubble number density of 10^{15} m^{-3} , H_2O -content-dependent non-Newtonian rheology, viscous dissipation, and a constant mass discharge rate of $10^{7.5} \text{ kg s}^{-1}$. The vertical axis is depth on all plots. (a) The change in magma pressure p_m due to magma-static and frictional pressure loss below the fragmentation depth. Above the fragmentation depth pressure loss is assumed to be linear (Koyaguchi, 2005). (b) Bubble volume fraction ϕ at the center of the conduit. (c) Bubble overpressure $p_g - p_m$ (solid line) and fragmentation threshold Δp_f (dashed line). Note the large increase in bubble overpressure at shallow depths until $p_g - p_m = \Delta p_f$, when fragmentation is predicted to occur (Spieler *et al.*, 2004). (d) Newtonian melt viscosity η_0 as a function of depth. Note the rapid viscosity increase at shallow depths due to H_2O exsolution, resulting in viscously limited bubble growth. (e) Viscous heating at the conduit wall becomes significant as viscosity increases, principally within a few hundred meters below the fragmentation depth.

4.7.4 Coupling the conduit and the magma chamber

The boundary conditions for the momentum equations at the bottom of the conduit can be a specified magma flux or specified pressure. Either may be transient because of changes in chamber pressure, in turn a consequence of magma withdrawal or replenishment, as well as compressibility of the vesicular magma and surrounding rock. A simple equation for chamber pressure is obtained by combining conservation of mass with an equation of state (Denlinger and Hoblitt, 1999; Wylie *et al.*, 1999)

$$\frac{dp}{dt} = \frac{1}{\rho\beta_e V} (Q_{in} - Q_{out}). \quad (4.46)$$

Here V is the volume of the magma chamber or conduit, Q_{in} is mass recharge rate, Q_{out} is mass discharge rate, and β_e is the effective compressibility. The latter incorporates both magma compressibility and wall-rock elasticity, and is usually much smaller than the compressibility of vesicular magma (Huppert and Woods, 2002; Woods *et al.*, 2006). Typically it is the feedbacks between magma chamber and conduit that result in complex and unsteady eruptive

$$\frac{\partial T}{\partial t} = \frac{\kappa}{\rho c_p} \left(\frac{\partial^2 T}{\partial r^2} + \frac{1}{r} \frac{\partial T}{\partial r} \right) - \frac{1}{\rho c_p} \left(\tau_{rz} \frac{\partial u_z}{\partial r} \right), \quad (4.45)$$

where c_p is the specific heat and κ is the thermal conductivity of the magma. The first term on the right-hand side accounts for diffusion of heat, and the last term represents viscous heating.

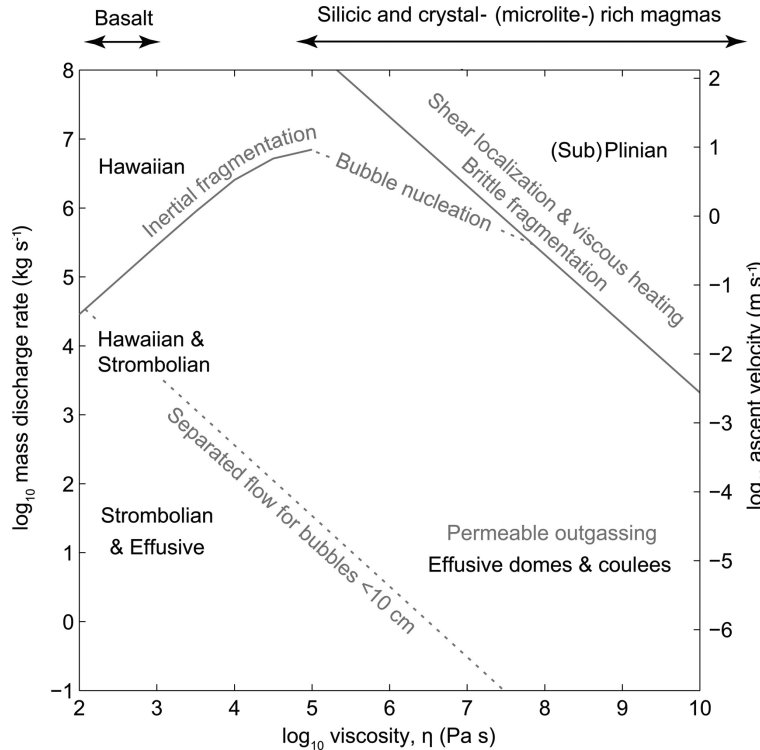


Figure 4.10 Summary of processes and mechanisms that govern magma flow in the volcanic conduit, based on modeling results and relations discussed in this chapter. Neglecting unsteady effects, discharge rate and viscosity control which processes have sufficient time to become dominant and affect eruption style.

behavior (Melnik and Sparks, 1999; Macedonio *et al.*, 2005).

4.8 What conduit models have taught us

Figure 4.10 shows the relationship between magma composition (in essence a proxy for viscosity), eruption rate (or equivalently ascent rate), and eruption style. The boundaries shown are not “hard” in that uncertainties in thresholds for fragmentation, unsteady flow, variation in volatile content, conduit geometry, two-dimensional flow, and crystallization are not addressed. Overall these boundaries are meant to provide insight into the conditions under which certain processes are expected to dominate and to illustrate their relationships with eruption style.

4.8.1 Subplinian and plinian eruptions

Subplinian and plinian eruptions are characterized by brittle magma fragmentation at mass

discharge rates on the order of 10^6 kg s^{-1} (subplinian) and 10^6 – 10^8 kg s^{-1} (plinian), sustained over several hours (Chapter 8). Syneruptive volatile exsolution and crystallization can lead to viscosity-limited bubble growth, large frictional pressure losses, and large decompression rates (Papale and Dobran, 1993, 1994), resulting in gas overpressure, supersaturation, and bubble nucleation (Massol and Koyaguchi, 2005), as well as fragmentation (Papale, 1999).

Whether fragmentation takes place depends on the conditions of magma ascent. However, fragmentation also feeds back on eruption dynamics. For example, the presence of pumice fragments after fragmentation, as opposed to complete fragmentation to ash, means that not all compressed gas contained in bubbles may be released, resulting in ascent velocities and pressures that are lower than if all gas were released. Incomplete outgassing of coarse fragments also increases the density of the erupting gas–pyroclast mixture, with consequences for the dynamics of the eruption column (Chapter 8, Papale, 2001). Furthermore, the granular stress

induced by >1 cm-size pyroclasts decreases exit velocities and enhances the lateral inhomogeneity in clast-size distribution throughout the conduit (Dufek and Bergantz, 2005).

The strong dependence of viscosity on temperature in silicic magmas is of considerable importance for shear heating near the conduit walls (Rosi *et al.*, 2004; Polacci *et al.*, 2005). The resulting viscosity reduction will change the flow profile toward a more plug-like flow and reduce frictional pressure loss. Consequently, the discharge rate increases for a given pressure drop between chamber and surface, and hence affects the depth of fragmentation and allows for multiple stable discharge rates (Costa and Macedonio, 2002; Mastin, 2005; Vedeneeva *et al.*, 2005; Costa *et al.*, 2007).

Eruption intensity may correlate with pre-eruptive H_2O content and magma composition (Papale *et al.*, 1998; Polacci *et al.*, 2004; Starostin *et al.*, 2005). However, changes in CO_2 content can have the opposite effect of H_2O (Papale and Polacci, 1999; Ongaro *et al.*, 2006). The transition from explosive to effusive eruptions in silicic magmas is thought to occur as magma ascent rates decrease, which allows more time for permeable outgassing and bubbles grow at near equilibrium conditions (Jaupart and Allegre, 1991; Woods and Koyaguchi, 1994; Gonnermann and Manga, 2007).

4.8.2 Strombolian eruptions

Typical strombolian eruptions (Chapter 6) consist of prolonged periods of impulsive explosions that typically eject 0.01 – 10 m^3 of pyroclastic material and volcanic gases at about 100 m s^{-1} . Mass balance considerations imply that much of the gas is derived from a larger volume of magma than is erupted, a consequence of slow magma ascent rates (<0.01 – 0.1 m s^{-1}). This permits significant bubble coalescence to form gas slugs and/or accumulations of bubbles, which decouple from the melt and rise to the surface where they burst. Aside from thermal modeling (Giberti *et al.*, 1992), some numerical conduit models that have dealt directly with details of strombolian eruptions are Wilson and Head (1981); Parfitt and Wilson (1995); James *et al.* (2008); O'Brian and Bean (2008); D'Auria

and Martini (2009); James *et al.* (2009); Pioli *et al.* (2009).

4.8.3 Hawaiian eruptions

Hawaiian eruptions are characterized by gas-rich fountains of basaltic magma sustained for hours to days at mass discharge rates of the order of 10^4 to $>10^6\text{ kg s}^{-1}$ (Houghton and Gonnermann, 2008). Fountains reach heights that exceed hundreds of meters producing ash and pyroclasts, presumably through hydrodynamic fragmentation (Namiki and Manga, 2008). Microtextural studies of pyroclasts indicate less open-system gas loss than for strombolian clasts (Polacci *et al.*, 2006).

Conduit models by Wilson and Head (1981) predict that magma ascent in hawaiian eruptions is homogeneous, with dispersed bubbles, so that rapid decompression and shallow H_2O exsolution lead to expansion-driven acceleration and the formation of a sustained magma fountain above the vent (Parfitt *et al.*, 1995; Parfitt, 2004). The transition from hawaiian to strombolian behavior is thought to occur at magma rise speeds of less than about 1 m s^{-1} , with a correlation between required rise speed and initial magmatic volatile content (Parfitt and Wilson, 1995). Alternatively, based on analog laboratory experiments it has been suggested that bubbles accumulate to form a magmatic foam, whose collapse produces an annular gas-melt flow within the conduit (Chapter 6; Jaupart and Vergnolle, 1988).

4.8.4 Effusive eruptions

Large volumes of basaltic magma often erupt effusively over prolonged periods of time, at rates up to 10^4 kg s^{-1} (Wolfe *et al.*, 1987). Silicic magmas of high viscosity may erupt effusively to form lava domes and coulees with time-averaged eruption rates ranging from 10^{-1} to 10^4 kg s^{-1} (Pyle, 2000). The resulting low ascent rates ($\Sigma 0.01\text{ m s}^{-1}$) are thought to facilitate permeable outgassing (Eichelberger *et al.*, 1986; Jaupart and Allegre, 1991; Woods and Koyaguchi, 1994; Massol and Jaupart, 1999). Sparks (1997) attributed the occurrence of time-dependent behavior during dome-forming eruptions to feedbacks associated with volatile-dependent magma viscosity, magma degassing, outgassing, and crystallization. Conduit models suggest that large

changes in discharge rate at relatively small changes in boundary conditions are the consequence of such feedbacks (Melnik and Sparks, 1999, 2005). They also demonstrate how non-linear feedbacks produce different steady discharge rates for the same boundary conditions but different initial conditions, perhaps explaining how transitions between effusive and explosive behavior occur (Melnik *et al.*, 2005; Clarke *et al.*, 2007).

For long-lived dome-forming eruptions, magma recharge is often treated as constant over part of the eruption. However, transient eruptive behavior can ensue as a direct consequence of compressibility of the vesicular magma and/or surrounding wall rock (Meriaux and Jaupart, 1995; Denlinger, 1997; Huppert and Woods, 2002; Costa *et al.*, 2007a). Feedbacks may be such that pressure build-up drives the system into a state where discharge rate exceeds recharge rate. With time, pressure decreases until the cycle repeats or is dynamically dampened toward a stable state (Barmin *et al.*, 2002). High shear stress at the conduit walls, in conjunction with shear-thinning rheology, may result in shear localization and brittle deformation and this may in turn enhance permeability and outgassing. Conduit models have also explored how brittle deformation may be associated with stick-slip behavior at the conduit walls and shallow seismicity, especially for magmas with high crystal content (Denlinger and Hoblitt, 1999; Goto, 1999; Collier and Neuberg, 2006; Iverson *et al.*, 2006; Hale, 2007).

subaerial flow, and incorporation of bubble nucleation.

- (2) The dynamics of magma flow within the volcanic conduit during strombolian and hawaiian eruptions remains controversial. The main challenge here is the modeling of the separated two-phase flow, where the topology of the flow can change drastically and rapidly in both space and time.
- (3) Magma flow in the volcanic conduit is affected by processes that occur over a wide range of length scales, from the fluid dynamics of magma ascent over kilometers to crystal/bubble nucleation and growth, as well as fragmentation over millimeter to micrometer scales. Accounting for these different scales requires the development of subgrid-type models capable of coupling explicit modeling of the various small-scale processes with fluid dynamical modeling of magma flow.
- (4) Eruption triggering is perhaps of foremost importance in terms of hazard mitigation. Integration of geodetic and remote-sensing observations with models of magma flow, supply, and storage is thus highly desirable. A major challenge is the incorporation of geological (tectonic and structural) complexities, which may require a departure for idealized one- or two-dimensional model geometries, as well as coupling between tectonically produced stresses and stresses within the magmatic system.

4.9 | Summary

Conduit models of magma ascent help us understand which mechanisms and processes are important for a broad range of effusive and dry explosive volcanic eruptions (Fig. 4.10). Some important open questions are:

- (1) What causes the observed unsteady behavior during sustained explosive eruptions? This will require models capable of exploring time-dependent dynamical feedbacks within the conduit, coupling between conduit and

4.10 | Notation

a	conduit radius (m)
A	cross-sectional area of conduit (m^2)
B	empirical constant
c	speed of sound in magma (m s^{-1})
c_p	specific heat ($\text{J kg}^{-1} \text{K}^{-1}$)
C_c	concentration of dissolved CO_2 (ppm)
C_i	mass fraction of dissolved volatile i
C_w	concentration of dissolved H_2O (wt.%)
D	diffusivity of dissolved volatile in melt ($\text{m}^2 \text{s}^{-1}$)
D_c	diffusivity of CO_2 dissolved in melt ($\text{m}^2 \text{s}^{-1}$)

D_i	diffusivity of dissolved volatile species i ($\text{m}^2 \text{s}^{-1}$)	Q_{in}	magma chamber mass recharge rate (kg s^{-1})
D_{wb}	diffusivity of H_2O dissolved in basalt melt ($\text{m}^2 \text{s}^{-1}$)	Q_{out}	magma chamber mass discharge rate (kg s^{-1})
D_{wr}	diffusivity of H_2O dissolved in rhyolite melt ($\text{m}^2 \text{s}^{-1}$)	Q_m	mass flow rate of melt phase (kg s^{-1})
f	friction factor for flow in a cylindrical pipe	r	radial distance from center of bubble or from center of conduit (m)
F_{wg}	wall drag force of the gas phase (N)	R	bubble radius (m)
F_{wm}	wall drag force of the melt phase (N)	S	radial distance from bubble center to midpoint of between adjacent bubbles (m)
g	acceleration due to gravity (m s^{-2})	t	time (s)
G_∞	shear modulus of melt (Pa)	T	temperature (K)
εG_D	activation energy for diffusion (J)	T_l	liquidus temperature (K)
εG^*	free energy for nucleus formation (J)	εT_e	undercooling of melt (K)
h	hindering function for Richardson-Zaki equation	u	magma velocity (m s^{-1})
H	specific enthalpy (J kg^{-1})	u_g	gas velocity (m s^{-1})
εH	change in enthalpy between melt and crystal (J)	u_m	melt velocity (m s^{-1})
I	homogeneous crystal nucleation rate ($\text{m}^{-3} \text{s}^{-1}$)	u_r	radial component of magma velocity (m s^{-1})
I_0	reference homogeneous crystal nucleation rate ($\text{m}^{-3} \text{s}^{-1}$)	u_z	vertical component of magma velocity (m s^{-1})
J	bubble nucleation rate ($\text{m}^{-3} \text{s}^{-1}$)	U_b	bubble ascent velocity (m s^{-1})
k	permeability (m^2)	U_m	ascent velocity of the melt phase (m s^{-1})
k_v	volumetric factor for Avrami equation	U_t	terminal rise velocity of a single bubble in infinite liquid (m s^{-1})
k_B	Boltzmann constant (J kg^{-1})	v	approach velocity of two bubbles or expansion velocity of vesicular magma (m s^{-1})
K	bulk viscosity (Pa s)	v_f	velocity in the melt film between bubbles (m s^{-1})
L	characteristic length scale for inertial fragmentation (m)	v_r	radial velocity of the melt surrounding a growing bubble (m s^{-1})
n	empirical coefficient	v_R	radial velocity of the melt-vapor interface of growing bubble (m s^{-1})
N_d	number of bubbles per volume of melt (m^{-3})	V	volume of magma chamber (m^3)
p	magma pressure (Pa)	Y	crystal growth rate (m s^{-1})
p_c	partial pressure of CO_2 (MPa)	Y_0	reference crystal growth rate (m s^{-1})
p_m	pressure of the melt (Pa)	z	vertical coordinate (m)
\dot{p}_m	melt decompression rate (Pa s^{-1})	α	empirical constant
p_g	pressure of the vapor inside bubbles (Pa)	β	empirical constant for Kozeny–Carman equation
p_w	partial pressure of H_2O (MPa)	β_e	effective compressibility ($\text{m}^2 \text{N}^{-1}$)
εp_f	critical gas overpressure for brittle fragmentation (Pa)	γ	vapor–melt surface tension (N m^{-1})
εp_s	supersaturation pressure of volatile in melt (Pa)	δ	empirical constant
Q	mass flow rate of magma (kg s^{-1})	ε	strain rate (s^{-1})
Q_g	mass flow rate of gas phase (kg s^{-1})	$\dot{\varepsilon}_f$	critical strain rate for structural failure of the melt (s^{-1})
Q_{gd}	mass flow rate of dissolve volatile phase (kg s^{-1})		

$\dot{\epsilon}_{st}$	strain rate at which shear thinning begins (s^{-1})
η	magma viscosity (Pa s)
η_0	Newtonian melt (liquid) viscosity (Pa s)
η_g	viscosity of vapor inside a bubble (Pa s)
η_r	Relative viscosity
θ	contact angle
κ	Thermal conductivity ($W K^{-1} m^{-1}$)
ρ	magma density ($kg m^{-3}$)
ρ_g	vapor density ($kg m^{-3}$)
ρ_m	melt density ($kg m^{-3}$)
σ	free energy of crystal–liquid interface (J)
τ_{dec}	characteristic decompression timescale (s)
τ_{dif}	characteristic diffusion time of volatile in melt (s)
τ_{if}	components of the stress tensor (Pa)
τ_r	viscous relaxation time (s)
τ_{vis}	characteristic viscous timescale (s)
ϕ_b	volume fraction of bubbles
ϕ_{bp}	percolation threshold
ϕ_x	volume fraction of crystals
ϕ_{xcr}	critical volume fraction of crystals
ϕ_{bcr}	critical volume fraction of bubbles
χ	empirical constant for Kozeny–Carman equation
ψ	geometrical factor
Ca	Capillary number, $\eta_0 \dot{\epsilon} R / \gamma$
Ca _{cr}	Capillary number at which bubbles break up, $\eta_0 \dot{\epsilon} R / \gamma$
M	Mach number, u^2 / c^2
Re	Reynolds number for flow in a cylindrical pipe, au_d / η
Re _b	Reynolds number for a growing bubble, $\dot{\epsilon} R^2 \rho / \eta_0$
Re _v	Reynolds number of expanding magma, $\rho(1 - \phi_b) v^2 L / (3\eta_0)$
We	Weber number, $2\rho v^2 R / \gamma$
We _{cr}	Weber number at which bubbles break up, $2\rho v^2 R / \gamma$
We _v	Weber number of expanding magma, $\rho(1 - \phi_b) v^2 L / \gamma$

Acknowledgments

The authors thank B. F. Houghton for stimulating discussions, as well as J. E. Hammer, L. Karlstrom, and M. Rudolph for constructive comments on

the manuscript. Both authors were supported by NSF while preparing this review.

References

- Alidibirov, M. (1994). A model for viscous magma fragmentation during volcanic blasts. *Bulletin of Volcanology*, **56**, 459–465.
- Allard, P., Burton, M. and Mure, F. (2005). Spectroscopic evidence for a lava fountain driven by previously accumulated magmatic gas. *Nature*, **433**, 407–410.
- Arbaret, L., Bystricky, M. and Champallier, R. (2007). Microstructures and rheology of hydrous synthetic magmatic suspensions deformed in torsion at high pressure. *Journal of Geophysical Research*, **112**.
- Bagdassarov, N. S. and Dingwell, D. B. (1992). A rheological investigation of vesicular rhyolite. *Journal of Volcanology and Geothermal Research*, **50**, 307–322.
- Bagdassarov, N., Dorfman, A. and Dingwell, D. B. (2000). Effect of alkalis, phosphorus, and water on the surface tension of haplogranite melt. *American Mineralogist*, **85**, 33–40.
- Barmin, A., Melnik, O. and Sparks, R. S. J. (2002). Periodic behavior in lava dome eruptions. *Earth and Planetary Science Letters*, **199**, 173–184.
- Batchelor, G. K. (1967). *An Introduction to Fluid Dynamics*. Cambridge: Cambridge University Press.
- Behrens, H. and Zhang, Y. X. (2001). Ar diffusion in hydrous silicic melts: implications for volatile diffusion mechanisms and fractionation. *Earth and Planetary Science Letters*, **192**, 363–376.
- Bird, R. B., Stewart, W. E. and Lightfoot, E. N. (1960). *Transport Phenomena*. New York: John Wiley.
- Blank, J. G. and Brooker, R. A. (1994). Experimental studies of carbon-dioxide in silicate melts; solubility, speciation, and stable carbon-isotope behavior. In M. R. Carroll and J. R. Holloway, (Eds.) *Volatiles in Magmas*, American Mineralogical Society, **30 Reviews in Mineralogy**, 157–186.
- Bluth, G. J. S., Schnetzler, C. C., Krueger, A. J. and Walter, L. S. (1993). The contribution of explosive volcanism to global atmospheric sulfur-dioxide concentrations. *Nature*, **366**, 327–329.
- Borrell, M. and Leal, L. G. (2008). Viscous coalescence of expanding low-viscosity drops; the dueling drops experiment. *Journal of Colloid and Interface Science*, **319**, 263–269.

- Boudon, G., Villemant, B., Komorowski, J. C., Ildefonse, P. and Semet, M. P. (1998). The hydrothermal system at Soufriere Hills volcano, Montserrat (West Indies): Characterization and role in the on-going eruption. *Geophysical Research Letters*, **25**, 3693–3696.
- Bourgue, E. and Richet, P. (2001). The effects of dissolved CO₂ on the density and viscosity of silicate melts: a preliminary study. *Earth and Planetary Science Letters*, **193**, 57–68.
- Brennen, C. E. (2005). *Fundamentals of Multiphase Flow*. New York: Cambridge University Press, 2nd edition.
- Bruce, P. M. and Huppert, H. E. (1989). Thermal control of basaltic fissure eruptions. *Nature*, **342**, 665–667.
- Caricchi, L., Burlini, L., Ulmer, P., et al. (2007). Non-Newtonian rheology of crystal-bearing magmas and implications for magma ascent dynamics. *Earth and Planetary Science Letters*, **264**, 402–419.
- Carman, P. C. (1956). *Flow of Gases Through Porous Media*. San Diego, CA: Academic.
- Carmichael, I. S. E. (2002). The andesite aqueduct: perspectives on the evolution of intermediate magmatism in west-central (105–99 degrees W) Mexico. *Contributions to Mineralogy Petrology*, **143**, 641–663.
- Carroll, M. R. and Webster, J. D. (1994). Solubilities of sulfur, noble-gases, nitrogen, chlorine, and fluorine in magmas. *Volatiles in Magmas*, **30**, 231–279.
- Clarke, A. B., Stephens, S., Teasdale, R., Sparks, R. S. J. and Diller, K. (2007). Petrologic constraints on the decompression history of magma prior to Vulcanian explosions at the Soufriere Hills volcano, Montserrat. *Journal of Volcanology and Geothermal Research*, **161**, 261–274.
- Collier, L. and Neuberg, J. (2006). Incorporating seismic observations into 2D conduit flow modeling. *Journal of Volcanology and Geothermal Research*, **152**, 331–346.
- Costa, A. and Macedonio, G. (2005). Viscous heating effects in fluids with temperature-dependent viscosity: Triggering of secondary flows. *Journal of Fluid Mechanics*, **540**, 21–38.
- Costa, A., Melnik, O. and Sparks, R. S. J. (2007). Controls of conduit geometry and wallrock elasticity on lava dome eruptions. *Earth and Planetary Science Letters*, **260**, 137–151.
- Costa, A., Melnik, O., Sparks, R. S. J. and Voight, B. (2007). Control of magma flow in dykes on cyclic lava dome extrusion. *Geophysical Research Letters*, **34**.
- Costa, A., Melnik, O. and Vedeneeva, E. (2007). Thermal effects during magma ascent in conduits. *Journal of Geophysical Research*, **112**.
- D'Auria, L. and Martini, M. (2009). Slug flow: Modeling in a conduit and associated elastic radiation. In R. A. Meyers, (Ed.) *Monitoring and mitigation of volcano hazards*, New York: Springer, 8153–8168.
- Denlinger, R. P. (1997). A dynamic balance between magma supply and eruption rate at Kilauea volcano, Hawaii. *Journal of Geophysical Research*, **102**, 18091–18100.
- Denlinger, R. P. and Hoblitt, R. P. (1999). Cyclic eruptive behavior of silicic volcanoes. *Geology*, **27**, 459–462.
- Dixon, J. E. (1997). Degassing of alkalic basalts. *American Mineralogist*, **82**, 368–378.
- Dobran, F. (1992). Nonequilibrium flow in volcanic conduits and application to the eruptions of Mt. St. Helens on May 18, 1980, and Vesuvius in A.D. 79. *Journal of Volcanology and Geothermal Research*, **49**, 285–311.
- Dobran, F. (2001). *Volcanic Processes Mechanisms in Material Transport*. New York, N Y: Kluwer Academic / Plenum Publishers.
- Dufek, J. and Bergantz, G. W. (2005). Transient two-dimensional dynamics in the upper conduit of a rhyolitic eruption: A comparison of closure models for the granular stress. *Journal of Volcanology and Geothermal Research*, **143**, 113–132.
- Edmonds, M., Oppenheimer, C., Pyle, D. M., Herd, R. A. and Thompson, G. (2003). SO₂ emissions from Soufriere Hills Volcano and their relationship to conduit permeability, hydrothermal interaction and degassing regime. *Journal of Volcanology and Geothermal Research*, **124**, 23–43.
- Eichelberger, J. C. (1995). Silicic volcanism. *Annual Reviews in Earth and Planetary Science*, **23**, 41–63.
- Eichelberger, J. C., Carrigan, C. R., Westrich, H. R. and Price, R. H. (1986). Non-explosive silicic volcanism. *Nature*, **323**, 598–602.
- Eposti Ongaro, T., Papale, P., Neri, A. and Del Seppia, D. (2006). Influence of carbon dioxide on the large-scale dynamics of magmatic eruptions at Phlegrean Fields (Italy). *Geophysical Research Letters*, **33**.
- Gardner, J. E. and Denis, M. H. (2004). Heterogeneous bubble nucleation on Fe-Ti oxide crystals in high-silica rhyolitic melts. *Geochimica et Cosmochimica Acta*, **68**, 3587–3597.
- Gardner, J. E. (2007). Heterogeneous bubble nucleation in highly viscous silicate melts during

- instantaneous decompression from high pressure. *Chemical Geology*, **236**, 1–12.
- Ghiaasiaan, S. M. (2008). *Two-Phase Flow, Boiling, and Condensation in Conventional and Miniature Systems*. New York: Cambridge University Press.
- Giberti, G. and Wilson, L. (1990). The influence of geometry on the ascent of magma in open fissures. *Bulletin of Volcanology*, **52**, 515–521.
- Giberti, G., Jaupart, C. and Sartoris, G. (1992). Steady-state operation of Stromboli Volcano, Italy: constraints on the feeding system. *Bulletin of Volcanology*, **54**, 535–541.
- Giordano, D. and Dingwell, D. B. (2003). Viscosity of hydrous Etna basalt: implications for Plinian-style basaltic eruptions. *Bulletin of Volcanology*, **65**, 8–14.
- Giordano, D., Russell, J. K. and Dingwell, D. B. (2008). Viscosity of magmatic liquids: A model. *Earth and Planetary Science Letters*, **271**, 123–134.
- Gonnermann, H. M. and Manga, M. (2003). Explosive volcanism may not be an inevitable consequence of magma fragmentation. *Nature*, **426**, 432–435.
- Gonnermann, H. M. and Manga, M. (2005a). Flow banding in obsidian: A record of evolving textural heterogeneity during magma deformation. *Earth and Planetary Science Letters*, **236**, 135–147.
- Gonnermann, H. M. and Manga, M. (2005b). Nonequilibrium magma degassing: Results from modeling of the ca.1340 AD eruption of Mono Craters, California. *Earth and Planetary Science Letters*, **238**, 1–16.
- Gonnermann, H. M. and Manga, M. (2007). The fluid mechanics inside a volcano. *Annual Reviews in Fluid Mechanics*, **39**, 321–356.
- Gonnermann, H. M. and Mukhopadhyay, S. (2007). Non-equilibrium degassing and a primordial source for helium in ocean-island volcanism. *Nature*, **449**, 1037–1040.
- Goto, A. (1999). A new model for volcanic earthquake at Unzen Volcano: Melt rupture model. *Geophysical Research Letters*, **26**, 2541–2544.
- Guet, S. and Ooms, G. (2006). Fluid mechanical aspects of the gas-lift technique. *Annual Reviews in Fluid Mechanics*, **38**, 225–249.
- Hale, A. J. (2007). Magma flow instabilities in a volcanic conduit: Implications for long-period seismicity. *Physics of the Earth and Planetary Interiors*, **163**, 163–178.
- Hale, A. J. and Muehlhaus, H. B. (2007). Modelling shear bands in a volcanic conduit: Implications for over-pressures and extrusion-rates. *Earth and Planetary Science Letters*, **263**, 74–87.
- Hammer, J. E. (2004). Crystal nucleation in hydrous rhyolite: Experimental data applied to classical theory. *American Mineralogist*, **89**, 1673–1679.
- Hauri, E. (2002). SIMS analysis of volatiles in silicate glasses, 2: isotopes and abundances in Hawaiian melt inclusions. *Chemical Geology*, **183**, 115–141.
- Hinze, J. O. (1955). Fundamentals of the hydrodynamic mechanisms of splitting in dispersion processes. *American Institute of Chemical Engineers Journal*, **1**, 289–295.
- Hirth, J. P., Pound, G. M. and St. Pierre, G. R. (1970). Bubble nucleation. *Metallurgical and Materials Transactions B*, **1**, 939–945.
- Houghton, B. F. and Gonnermann, H. M. (2008). Basaltic explosive volcanism: constraints from deposits and models. *Chemie der Erde – Geochemistry*, **68**, 117–140.
- Hui, H. J. and Zhang, Y. X. (2007). Toward a general viscosity equation for natural anhydrous and hydrous silicate melts. *Geochimica et Cosmochimica Acta*, **71**, 403–416.
- Huppert, H. E. and Woods, A. W. (2002). The role of volatiles in magma chamber dynamics. *Nature*, **420**, 493–495.
- Hurwitz, S. and Navon, O. (1994). Bubble nucleation in rhyolitic melts: Experiments at high-pressure, temperature, and water content. *Earth and Planetary Science Letters*, **122**, 267–280.
- Ittai, K., Lyakhovskiy, V. and Navon, O. (2010). Bubble growth in visco-elastic magma: Implications to magma fragmentation and bubble nucleation. *Bulletin of Volcanology*, **73**, 39–54.
- Iverson, R. M., Dzurisin, D., Gardner, C. A. et al. (2006). Dynamics of seismogenic volcanic extrusion at Mount St Helens in 2004–05. *Nature*, **444**, 439–443.
- James, M. R., Lane, S. J. and Corder, S. B. (2008). Modelling the rapid near-surface expansion of gas slugs in low viscosity magmas. In S. J. Lane and J. S. Gilbert, (Eds.) *Fluid Motion in Volcanic Conduits: A Source of Seismic and Acoustic Signals*, Geological Society of London Special Publication, **307**, 147–167.
- James, M. R., Lane, S. J., Wilson, L. and Corder, S. B. (2009). Degassing at low magma-viscosity volcanoes: Quantifying the transition between passive bubble-burst and Strombolian eruption. *Journal of Volcanology and Geothermal Research*, **180**, 81–88.
- James, P. F. (1985). Kinetics of crystal nucleation in silicate glasses. *Journal of Non-Crystalline Solids*, **73**, 517–540.

- Jaupart, C. and Allegre, C. J. (1991). Gas content, eruption rate and instabilities of eruption regime in silicic volcanoes. *Earth and Planetary Science Letters*, **102**, 413–429.
- Jaupart, C. and Vergnolle, S. (1988). Laboratory models of Hawaiian and Strombolian eruptions. *Nature*, **331**, 58–60.
- Johnson, M. C., Anderson, A. T. and Rutherford, M. J. (1994). Pre-eruptive volatile contents of magmas. In *Volatiles In Magmas*, Washington D. C.: Mineralogical Society of America, **30 Reviews In Mineralogy**, 281–330.
- Kennedy, B., Spieler, O., Scheu, B. *et al.* (2005). Conduit implosion during Vulcanian eruptions. *Geology*, **33**, 581–584.
- Kerrick, D. M. and Jacobs, G. K. (1981). A modified Redlich-Kwong Equation for H₂O, CO₂, and H₂O-CO₂ mixtures at elevated pressures and temperatures. *American Journal of Science*, **281**, 735–767.
- Klug, C. and Cashman, K. V. (1996). Permeability development in vesiculating magmas: implications for fragmentation. *Bulletin of Volcanology*, **58**, 87–100.
- Koyaguchi, T. (2005). An analytical study for 1-dimensional steady flow in volcanic conduits. *Journal of Volcanology and Geothermal Research*, **143**, 29–52.
- Lange, R. A. (1994). The effect of H₂O, CO₂ and F on the density and viscosity of silicate melts. *Reviews in Mineralogy*, **30**, 331–369.
- Lavallee, Y., Hess, K. U., Cordonnier, B. and Dingwell, D. B. (2007). Non-Newtonian rheological law for highly crystalline dome lavas. *Geology*, **35**, 843–846.
- Lejeune, A. M., Bottinga, Y., Trull, T. W. and Richet, P. (1999). Rheology of bubble-bearing magmas. *Earth and Planetary Science Letters*, **166**, 71–84.
- Lejeune, A. M. and Richet, P. (1995). Rheology of crystal-bearing silicate melts – An experimental study at high viscosities. *Journal of Geophysical Research*, **100**, 4215–4229.
- Lensky, N. G., Navon, O. and Lyakhovsky, V. (2004). Bubble growth during decompression of magma: experimental and theoretical investigation. *Journal of Volcanology and Geothermal Research*, **129**, 7–22.
- Liu, Y., Zhang, Y. X. and Behrens, H. (2005). Solubility of H₂O in rhyolitic melts at low pressures and a new empirical model for mixed H₂O-CO₂ solubility in rhyolitic melts. *Journal of Volcanology and Geothermal Research*, **143**, 219–235.
- Llewellyn, E. W. and Manga, A. (2005). Bubble suspension rheology and implications for conduit flow. *Journal of Volcanology and Geothermal Research*, **143**, 205–217.
- Macedonio, G., Dobran, F. and Neri, A. (1994). Erosion processes in volcanic conduits and application to the AD 79 eruption of Vesuvius. *Earth and Planetary Science Letters*, **121**, 137–152.
- Macedonio, G., Neri, A., Marti, J. and Folch, A. (2005). Temporal evolution of flow conditions in sustained magmatic explosive eruptions. *Journal of Volcanology and Geothermal Research*, **143**, 153–172.
- Manga, M., Castro, K. V., Cashman, K. V. and Loewenberg, M. (1998). Rheology of bubble-bearing magmas: Theoretical results. *Journal of Volcanology and Geothermal Research*, **87**, 15–28.
- Manga, M. and Stone, H. A. (1994). Interactions between bubbles in magmas and lavas: Effects of bubble deformation. *Journal of Volcanology and Geothermal Research*, **63**, 267–279.
- Mangan, M. and Sisson, T. (2000). Delayed, disequilibrium degassing in rhyolite magma: Decompression experiments and implications for explosive volcanism. *Earth and Planetary Science Letters*, **183**, 441–455.
- Mangan, M. and Sisson, T. (2005). Evolution of melt-vapor surface tension in silicic volcanic systems: Experiments with hydrous melts. *Journal of Geophysical Research*, **110**, doi:10.1029/2004JB003215.
- Marsh, B. D. (1998). On the interpretation of crystal size distributions in magmatic systems. *J. Petrol.*, **39**, 553–599.
- Marti, J., Soriano, C. and Dingwell, D. B. (1999). Tube pumices as strain markers of the ductile-brittle transition during magma fragmentation. *Nature*, **402**, 650–653.
- Martula, D. S., Hasegawa, T., Lloyd, D. R. and Bonnecaze, R. T. (2000). Coalescence-induced coalescence of inviscid droplets in a viscous fluid. *Journal of Colloid and Interface Science*, **232**, 241–253.
- Massol, H. and Jaupart, C. (1999). The generation of gas overpressure in volcanic eruptions. *Earth and Planetary Science Letters*, **166**, 57–70.
- Massol, H., Jaupart, C. and Pepper, D. W. (2001). Ascent and decompression of viscous vesicular magma in a volcanic conduit. *Journal of Geophysical Research*, **106**, 16223–16240.
- Massol, H. and Koyaguchi, T. (2005). The effect of magma flow on nucleation of gas bubbles in a volcanic conduit. *Journal of Volcanology and Geothermal Research*, **143**, 69–88.

- Mastin, L. G. (1995). Thermodynamics of gas and steam-blast eruptions. *Bulletin of Volcanology*, **57**, 85–98.
- Mastin, L. G. (2005). The controlling effect of viscous dissipation on magma flow in silicic conduits. *Journal of Volcanology and Geothermal Research*, **143**, 17–28.
- Mastin, L. G. and Ghiorso, M. S. (2000). A numerical program for steady-state flow of magma-gas mixtures through vertical eruptive conduits. United States Geological Survey, 00–209 *Open-File Report*, **53**.
- McMillan, P. F. (1994). Water solubility and speciation models. In M. R. Carroll and J. R. Holloway, (Eds.) *Volatiles in Magmas*, Mineralogical Society of America, **30 Reviews in Mineralogy**, 131–156.
- Melnik, O., Barmin, A. A. and Sparks, R. S. J. (2005). Dynamics of magma flow inside volcanic conduits with bubble overpressure buildup and gas loss through permeable magma. *Journal of Volcanology and Geothermal Research*, **143**, 53–68.
- Melnik, O. and Sparks, R. S. J. (1999). Nonlinear dynamics of lava dome extrusion. *Nature*, **402**, 37–41.
- Melnik, O. and Sparks, R. S. J. (2005). Controls on conduit magma flow dynamics during lava dome building eruptions. *Journal of Geophysical Research*, **110**.
- Meriaux, C. and Jaupart, C. (1995). Simple fluid dynamic models of volcanic rift zones. *Earth and Planetary Science Letters*, **136**, 223–240.
- Mitchell, K. L. (2005). Coupled conduit flow and shape in explosive volcanic eruptions. *Journal of Volcanology and Geothermal Research*, **143**, 187–203.
- Moynihan, C. T. (1995). Structural relaxation and the glass transition. *Reviews in Mineralogy and Geochemistry*, **32**, 1–19.
- Mueller, S., Scheu, B., Spieler, O. and Dingwell, D. B. (2008). Permeability control on magma fragmentation. *Geology*, **36**, 399–402.
- Muller, R., Zanutto, E. D. and Fokin, V. M. (2000). Surface crystallization of silicate glasses: nucleation sites and kinetics. *Journal of Non-Crystalline Solids*, **274**, 208–231.
- Namiki, A. and Manga, M. (2005). Response of a bubble bearing viscoelastic fluid to rapid decompression: Implications for explosive volcanic eruptions. *Earth and Planetary Science Letters*, **236**, 269–284.
- Namiki, A. and Manga, M. (2008). Transition between fragmentation and permeable outgassing of low viscosity magmas. *Journal of Volcanology and Geothermal Research*, **169**, 48–60.
- Newman, S. and Lowenstern, J. B. (2002). VOLATILECALC: A silicate melt-H₂O-CO₂ solution model written in Visual Basic for Excel. *Comp. Geosci.*, **28**, 597–604.
- Nowak, M., Schreen, D. and Spickenbom, K. (2004). Argon and CO₂ on the race track in silicate melts: A tool for the development of a CO₂, speciation and diffusion model. *Geochimica et Cosmochimica Acta*, **68**, 5127–5138.
- O'Brian, G. S. and Bean, C. J. (2008). Seismicity on volcanoes generated by gas slug ascent. *Geophysical Research Letters*, **35**, L16308, doi: 10.1029/2008gl035001.
- Okumura, S., Nakamura, M., Nakano, T., Uesugi, K. and Tsuchiyama, K. (2010). Shear deformation experiments on vesicular rhyolite: Implications for brittle fracturing, degassing, and compaction of magmas in volcanic conduits. *Journal of Geophysical Research*, **115**, doi:10.1029/2009JB006904.
- Okumura, S., Nakamura, M., Tsuchiyama, K., Nakano, T. and Uesugi, K. (2008). Evolution of bubble microstructure in sheared rhyolite: Formation of a channel-like bubble network. *Journal of Geophysical Research*, **113**, doi:10.1029/2007JB005362.
- Pal, R. (2003). Rheological behavior of bubble-bearing magmas. *Earth and Planetary Science Letters*, **207**, 165–179.
- Papale, P. (1999). Strain-induced magma fragmentation in explosive eruptions. *Nature*, **397**, 425–428.
- Papale, P. (2001). Dynamics of magma flow in volcanic conduits with variable fragmentation efficiency and nonequilibrium pumice degassing. *Journal of Geophysical Research*, **106**, 11043–11065.
- Papale, P. (2005). Determination of total H₂O and CO₂ budgets in evolving magmas from melt inclusion data. *Journal of Geophysical Research*, **110**.
- Papale, P. and Dobran, F. (1993). Modeling of the ascent of magma during the Plinian eruption of Vesuvius in AD 79. *Journal of Volcanology and Geothermal Research*, **58**, 101–132.
- Papale, P. and Dobran, F. (1994). Magma flow along the volcanic conduit during the Plinian and pyroclastic flow phases of the May 18, 1980, Mount-St. Helens eruption. *Journal of Geophysical Research*, **99**, 4355–4373.
- Papale, P., Moretti, R. and Barbato, D. (2006). The compositional dependence of the saturation surface of H₂O+CO₂ fluids in silicate melts. *Chemical Geology*, **229**, 78–95.
- Papale, P., Neri, A. and Macedonio, G. (1998). The role of magma composition and water content in explosive eruptions – 1. Conduit ascent dynamics. *Journal of Volcanology and Geothermal Research*, **87**, 75–93.

- Papale, P. and Polacci, M. (1999). Role of carbon dioxide in the dynamics of magma ascent in explosive eruptions. *Bulletin of Volcanology*, **60**, 583–594.
- Parfitt, E. A. (2004). A discussion of the mechanisms of explosive basaltic eruptions. *Journal of Volcanology and Geothermal Research*, **134**, 77–107.
- Parfitt, E. A. and Wilson, L. (1995). Explosive volcanic eruptions – IX. The transition between Hawaiian-style lava fountaining and Strombolian explosive activity. *Geophysical Journal International*, **121**, 226–232.
- Parfitt, E. A., Wilson, L. and Neal, C. A. (1995). Factors influencing the height of Hawaiian lava fountains: Implications for the use of fountain height as an indicator of magma gas content. *Bulletin of Volcanology*, **57**, 440–450.
- Pioli, L., Azzopardi, B. J. and Cashman, K. V. (2009). Controls on the explosivity of scoria cone eruptions: Magma segregation at conduit junctions. *Journal of Volcanology and Geothermal Research*, **186**, 407–415.
- Polacci, M., Corsaro, R. A. and Andronico, D. (2006). Coupled textural and compositional characterization of basaltic scoria: Insights into the transition from Strombolian to fire fountain activity at Mount Etna, Italy. *Geology*, **34**, 201–204.
- Polacci, M., Papale, P., Del Seppia, D., Giordano, D. and Romano, C. (2004). Dynamics of magma ascent and fragmentation in trachytic versus rhyolitic eruptions. *Journal of Volcanology and Geothermal Research*, **131**, 93–108.
- Polacci, M., Rosi, M., Landi, P., Di Muro, A. and Papale, P. (2005). Novel interpretation for shift between eruptive styles in some volcanoes. *Eos, Transactions, American Geophysical Union*, **86**, 333–336.
- Press, W. H., Teukolsky, S. A., Vetterling, W. T. and Flannery, B. P. (1992). *Numerical Recipes in C: The Art of Scientific Computing*. Cambridge: Cambridge University Press.
- Proussevitch, A., Sahagian, D. and Anderson, A. (1993a). Dynamics of diffusive bubble growth in magmas: Isothermal case. *Journal of Geophysical Research*, **98**, 22,283–22,307.
- Proussevitch, A. A. and Sahagian, D. L. (1998). Dynamics and energetics of bubble growth in magmas: Analytical formulation and numerical modeling. *Journal of Geophysical Research*, **103**, 18223–18251.
- Proussevitch, A. A., Sahagian, D. L. and Kutolin, V. A. (1993b). Stability Of Foams In Silicate Melts. *Journal of Volcanology and Geothermal Research*, **59**, 161–178.
- Pyle, D. M. (2000). Sizes of volcanic eruptions. In B. F. Houghton, H. Rymer, J. Stix, S. McNutt and H. Sigurdsson, (Eds.) *Encyclopedia of Volcanoes*, San Diego: Academic Press, 263–269.
- Pyle, D. M. and Pyle, D. L. (1995). Bubble migration and the initiation of volcanic eruptions. *Journal of Volcanology and Geothermal Research*, **67**, 227–232.
- Richardson, J. F. and Zaki, W. N. (1954). The sedimentation of a suspension of uniform spheres under conditions of viscous flow. *Chemical Engineering Science*, **3**, 65–73.
- Rosi, M., Landi, P., Polacci, M., Di Muro, A. and Zandomenighi, D. (2004). Role of conduit shear on ascent of the crystal-rich magma feeding the 800-year- BP Plinian eruption of Quilotoa Volcano (Ecuador). *Bulletin of Volcanology*, **66**, 307–321.
- Rosner, D. E. and Epstein, M. (1972). Effects of interface kinetics, capillarity and solute diffusion on bubble growth rates in highly supersaturated liquids. *Chemical Engineering Science*, **27**, 69–88.
- Rust, A. C. and Cashman, K. V. (2004). Permeability of vesicular silicic magma: Inertial and hysteresis effects. *Earth and Planetary Science Letters*, **228**, 93–107.
- Rust, A. C., Manga, M. and Cashman, K. V. (2003). Determining flow type, shear rate and shear stress in magmas from bubble shapes and orientations. *Journal of Volcanology and Geothermal Research*, **122**, 111–132.
- Saar, M. O. and Manga, M. (1999). Permeability-porosity relationship in vesicular basalts. *Geophysical Research Letters*, **26**, 111–114.
- Sahagian, D. (2005). Volcanic eruption mechanisms: Insights from intercomparison of models of conduit processes. *Journal of Volcanology and Geothermal Research*, **143**, 1–15.
- Sahagian, D. L. and Proussevitch, A. A. (1996). Thermal effects of magma degassing. *Journal of Volcanology and Geothermal Research*, **74**, 19–38.
- Scriven, L. E. (1959). On the dynamics of phase growth. *Chemical Engineering Science*, **10**, 1–13.
- Seyfried, R. and Freundt, A. (2000). Experiments on conduit flow and eruption behavior of basaltic volcanic eruptions. *Journal of Geophysical Research*, **105**, 23727–23740.
- Shimozuru, D. (1994). Physical parameters governing the formation of Pele's hair and tears. *Bulletin of Volcanology*, **56**, 217–219.
- Slezin, Y. B. (2003). The mechanism of volcanic eruptions (a steady state approach). *Journal of Volcanology and Geothermal Research*, **122**, 7–50.

- Sparks, R. S. J. (1978). The dynamics of bubble formation and growth in magmas: A review and analysis. *Journal of Volcanology and Geothermal Research*, **3**, 1–37.
- Sparks, R. S. J. (1997). Causes and consequences of pressurisation in lava dome eruptions. *Earth and Planetary Science Letters*, **150**, 177–189.
- Sparks, R. S. J., Barclay, J., Jaupart, C., Mader, H. M. and Phillips, J. C. (1994). Physical aspects of magmatic degassing I. Experimental and theoretical constraints on vesiculation. In *Volatiles In Magmas*, Washington D. C.: Mineralogical Society of America, **30 Reviews In Mineralogy**, 413–445.
- Spieler, O., Kennedy, B., Kueppers, U. et al. (2004). The fragmentation threshold of pyroclastic rocks. *Earth and Planetary Science Letters*, **226**, 139–148.
- Spohn, T., Hort, M. and Fischer, H. (1988). Numerical simulation of the crystallization of multicomponent melts in thin dikes or sills. 1. The liquidus phase. *Journal of Geophysical Research*, **93**, 4880–4894.
- Starostin, A. B., Barmin, A. A. and Melnik, O. E. (2005). A transient model for explosive and phreatomagmatic eruptions. *Journal of Volcanology and Geothermal Research*, **143**, 133–151.
- Stein, D. J. and Spera, F. J. (2002). Shear viscosity of rhyolite-vapor emulsions at magmatic temperatures by concentric cylinder rheometry. *Journal of Volcanology and Geothermal Research*, **113**, 243–258.
- Stevenson, R. J., Dingwell, D. B., Webb, S. L. and Sharp, T. G. (1996). Viscosity of microlite-bearing rhyolitic obsidians: An experimental study. *Bulletin of Volcanology*, **58**, 298–309.
- Tait, S., Jaupart, C. and Vergnolle, S. (1989). Pressure, gas content and eruption periodicity of a shallow, crystallizing magma chamber. *Earth and Planetary Science Letters*, **92**, 107–123.
- Takeuchi, S., Nakashima, S., Tomiya, A. and Shinohara, H. (2005). Experimental constraints on the low gas permeability of vesicular magma during decompression. *Geophysical Research Letters*, **32**.
- Taylor, G. I. (1932). The viscosity of a fluid containing small drops of another fluid. *Proceedings of the Royal Society of London A: Mathematical, Physical & Engineering Sciences*, **138**, 41–48.
- Thies, M. (2002). *Herstellung und rheologische Eigenschaften von porösen Kalk-Natron-Silicatschmelzen*. Ph. d., RU.
- Thomas, N., Jaupart, C. and Vergnolle, S. (1994). On the vesicularity of pumice. *Journal of Geophysical Research*, **99**, 15633–15644.
- Toramaru, A. (1989). Vesiculation process and bubble-size distributions In ascending magmas with constant velocities. *Journal of Geophysical Research*, **94**, 17523–17542.
- Tuffen, H., Dingwell, D. B. and Pinkerton, H. (2003). Repeated fracture and healing of silicic magma generate flow banding and earthquakes? *Geology*, **31**, 1089–1092.
- Vedeneeva, E. A., Melnik, O. E., Barmin, A. A. and Sparks, R. S. J. (2005). Viscous dissipation in explosive volcanic flows. *Geophysical Research Letters*, **32**.
- Verhoogen, J. (1951). Mechanics of ash formation. *American Journal of Science*, **249**, 729–739.
- Villermaux, E. (2007). Fragmentation. *Annual Reviews in Fluid Mechanics*, **39**, 419–446.
- Wallace, P. J. (2005). Volatiles in subduction zone magmas: concentrations and fluxes based on melt inclusion and volcanic gas data. *Journal of Volcanology and Geothermal Research*, **140**, 217–240.
- Wallace, P. J., Carn, S. A. R., William, I., Bluth, G. J. S. and Gerlach, T. M. (2003). Integrating petrologic and remote sensing perspectives on magmatic volatiles and volcanic degassing. *Eos, Transactions, American Geophysical Union*, **84**, 446–447.
- Wallis, G. B. (1969). *One-Dimensional Two-phase Flow*. McGraw-Hill.
- Watson, E. B. (1994). Diffusion in volatile-bearing magmas. *Reviews in Mineralogy*, **30**, 371–411.
- Webb, S. (1997). Silicate melts: Relaxation, rheology, and the glass transition. *Reviews of Geophysics*, **35**, 191–218.
- Wilson, L. and Head, J. W. (1981). Ascent and eruption of basaltic magma on the Earth and Moon. *Journal of Geophysical Research*, **86**, 2971–3001.
- Wilson, L., Sparks, R. S. J. and Walker, G. P. L. (1980). Explosive volcanic eruptions – IX. The control of magma properties and conduit geometry on eruption column behavior. *Geophysical Journal of the Royal Astronomical Society*, **63**, 117–148.
- Wolfe, E. W., Garcia, M. O., Jackson, D. B. et al. (1987). The Pu'u O'o eruption of Kilauea Volcano, episodes 1–20, January 3, 1983, to June 8, 1984. In Decker, R. W. and Wright, T. L. and Stauffer, P. H., (Ed.) *Volcanism in Hawaii*, United States Geological Survey, **1350 United States Geological Survey Professional Paper**, 471–508.
- Woods, A. W., Bokhove, O., de Boer, A. and Hill, B. E. (2006). Compressible magma flow in a two-dimensional elastic-walled dike. *Earth and Planetary Science Letters*, **246**, 241–250.

- Woods, A. W. and Cardoso, S. S. S. (1997). Triggering basaltic volcanic eruptions by bubble-melt separation. *Nature*, **385**, 518–520.
- Woods, A. W. and Koyaguchi, T. (1994). Transitions between explosive and effusive eruption of silicic magmas. *Nature*, **370**, 641–644.
- Wright, H. M. N., Cashman, K. V., Gottesfeld, E. H. and Roberts, J. J. (2009). Pore structure of volcanic clasts: Measurements of permeability and electrical conductivity. *Earth and Planetary Science Letters*, **280**.
- Wylie, J. J. and Lister, J. R. (1995). The effects of temperature-dependent viscosity on flow in a cooled channel with application to basaltic fissure eruptions. *Journal of Fluid Mechanics*, **305**, 239–261.
- Wylie, J. J., Voight, B. and Whitehead, J. A. (1999). Instability of magma flow from volatile-dependent viscosity. *Science*, **285**, 1883–1885.
- Zenit, R., Koch, D. L. and Sangani, A. S. (2001). Measurements of the average properties of a suspension of bubbles rising in a vertical channel. *Journal of Fluid Mechanics*, **429**, 307–342.
- Zhang, Y. X. (1999). A criterion for the fragmentation of bubbly magma based on brittle failure theory. *Nature*, **402**, 648–650.
- Zhang, Y. X. and Behrens, H. (2000). H₂O diffusion in rhyolitic melts and glasses. *Chemical Geology*, **169**, 243–262.
- Zhang, Y. X., Xu, Z. J., Zhu, M. F. and Wang, H. Y. (2007). Silicate melt properties and volcanic eruptions. *Reviews of Geophysics*, **45**.
- Zimanowski, B., Buttner, R., Lorenz, V. and Hafele, H. G. (1997). Fragmentation of basaltic melt in the course of explosive volcanism. *Journal of Geophysical Research*, **102**, 803–814.
- Zimanowski, B., Wohletz, K., Dellino, P. and Buttner, R. (2003). The volcanic ash problem. *Journal of Volcanology and Geothermal Research*, **122**, 1–5.

Exercises

Consider two magmas, a basalt ($\eta = 1 \text{ Pa s}$, $\rho = 2800 \text{ kg m}^{-3}$) and rhyolite ($\eta = 10^6 \text{ Pa s}$, $\rho = 2600 \text{ kg m}^{-3}$), rising in a conduit. Assume a conduit radius of 10 m and 1 m for the rhyolite and basalt, respectively. Assume a pressure gradient driving magma ascent of 500 Pa m^{-1} . For both cases:

- 4.1 Calculate the velocity as a function of radial position in the conduit.
- 4.2 Evaluate the strain rates at the conduit walls. Are the strain rates large enough that the melt might be shear-thinning or undergo structural failure?
- 4.3 Calculate the capillary number for a 1 cm radius bubble. Will the bubbles become deformed by the ascending magma?
- 4.4 Calculate the rise speed of a 1 cm bubble relative to the surrounding melt. Given this speed, what flow regime is likely to characterize the magma (see Fig. 4.4).